eLife

Reviewed Preprint
v2 • September 12, 2025
Revised by authors

Reviewed Preprint
v1 • April 11, 2025

Neuroscience

Regional heterogeneities of oligodendrocytes underlie biased Ranvier node spacing along single axons in sound localization circuit

Ryo Egawa, Kota Hiraga, Ryosuke Matsui, Dai Watanabe, Hiroshi Kuba

Department of Cell Physiology, Graduate School of Medicine, Nagoya University, Nagoya, Japan • Department of Biological Sciences, Graduate School of Medicine, Kyoto University, Kyoto, Japan

https://en.wikipedia.org/wiki/Open_access

Copyright information

eLife Assessment

This **important** study uses the delay line axon model in the chick brainstem auditory circuit to examine the interactions between oligodendrocytes and axons in the formation of internodal distances. This is a significant and actively studied topic, and the authors have used this preparation to support the hypothesis that regional heterogeneity in oligodendrocytes underlies the observed variation in internodal length. In a **solid** series of experiments, the authors have used enhanced tetanus neurotoxin light chains, a genetically encoded silencing tool, to inhibit vesicular release from axons and support the hypothesis that regional heterogeneity among oligodendrocytes may underlie the biased nodal spacing pattern in the sound localization circuit.

[Editors' note: this paper was reviewed by Review Commons.]

https://doi.org/10.7554/eLife.106415.2.sa3

Abstract

Spacing of Ranvier nodes along myelinated axons is a critical determinant of conduction velocity, influencing spike arrival timing and hence neural circuit function. In the chick brainstem auditory circuit, the pattern of nodal spacing varies regionally along single axons, enabling precise binaural integration for sound localization. Using this model, we investigated the potential factors underlying the biased nodal spacing pattern. 3D morphometry revealed that these axons were almost fully myelinated by oligodendrocytes exhibiting distinct morphologies and cell densities across regions after hearing onset. The structure of axons did not affect internodal length. Inhibiting vesicular release from the axons did not affect internodal length or oligodendrocyte morphology, but caused unmyelinated segments on the axons by suppressing oligodendrogenesis near the presynaptic terminals. These results suggest that the regional heterogeneity in the intrinsic properties of oligodendrocytes is a prominent determinant of the biased nodal spacing pattern in the sound localization circuit, while activity-dependent signaling supports the

pattern by ensuring adequate oligodendrocyte density. Our findings highlight the importance of oligodendrocyte heterogeneity in fine-tuning neural circuit function.

Introduction

Ranvier nodes are highly excitable domains distributed along myelinated axons and contribute to increase conduction velocity through saltatory conduction. The distance between adjacent nodes (internodal length) affects the speed of saltatory conduction, with longer internodes leading to faster conduction, and hence has a significant impact on neural circuit function by influencing the timing of input arrival at target neurons. The pattern of nodal spacing along axons is not necessarily uniform. Recent studies have shown that the internodal length varies not only among axonal types and brain regions (Chong et al., 2012), but also along individual axons (Tomassy et al., 2014; Ford et al., 2015; Bonetto et al., 2021). Despite its potential importance in neural information processing, the mechanisms regulating nodal spacing patterns are not well understood (Normand and Rasband, 2016).

Various factors could contribute to the emergence of nodal spacing patterns along axons. In the central nervous system (CNS), each Ranvier node is formed through the following processes. Immature oligodendrocytes contact axons with their processes, initiating myelin formation that extends along the axon (Snaidero et al., 2014). At the ends of the extending myelin, the paranodal domain, at which the myelin tip contacts the axon, acts as a diffusion barrier and facilitates the clustering of voltage-gated sodium channels (Nav) and the scaffolding protein ankyrinG (AnkG) to form a heminode. Subsequent restriction of the gap between two neighboring heminodes forms a mature Ranvier node (Vabnick et al., 1996; Susuki et al., 2013; Rasband and Peles, 2015; 2021). Thus, the patterning of nodal spacing along axons is based on multicellular interactions among oligodendrocytes and axons and could be influenced by multiple factors associated with these cells, the factors related to oligodendrocytes include their morphological characteristics (e.g., the number and length of myelin sheaths) and cell density relative to axons (Chong et al., 2012), while those related to axons include their branching (Stedehouder et al., 2019), diameter (Bechler et al., 2015), and neural activity (Fields, 2015; Bechler et al., 2018; Bonetto et al., 2021; Osanai et al., 2022). In addition, the contributions of these factors would vary significantly due to the diversity of both cell types and developmental stages, which obscures our understanding of the mechanisms of determining the nodal spacing patterns.

To understand the regulatory mechanisms of nodal spacing, the chicken brainstem auditory circuit is an excellent model, because the nodal spacing is biased in a region-dependent manner along the same projecting axons, minimizing the effects of neuronal diversity. In addition, this regional difference in internodal length is also important in the computation of neural circuits for sound localization. Sound localization is the ability to identify the direction of sound source and involves detecting the time difference in sound arrivals between the ears (interaural time difference, ITD) in the order of microseconds. The ITD detection is mediated by an array of coincidence detector neurons in the nucleus laminaris (NL) that receive excitatory synaptic inputs from both sides of the nucleus magnocellularis (NM), a homologue of mammalian anteroventral cochlear nucleus (**Figure 1A**) (Carr and Konishi, 1990; Hyson 2005). In this circuit, the spacing of nodes along the axon of NM neurons differs among regions; the internodal length is longer at the tract region across the midline than at other regions including the NL (**Figure 1B**) (Seidl et al., 2010). The long internodes reduce the conduction time from the contralateral side and compensate for the difference in axonal pathlengths between the two sides (Seidl et al., 2014), while the short internodes expand the dynamic range for detectable ITD within the NL. Therefore, this model will be an important stepping stone for elucidating the regulatory mechanisms of nodal spacing and their impact on neural circuit function.

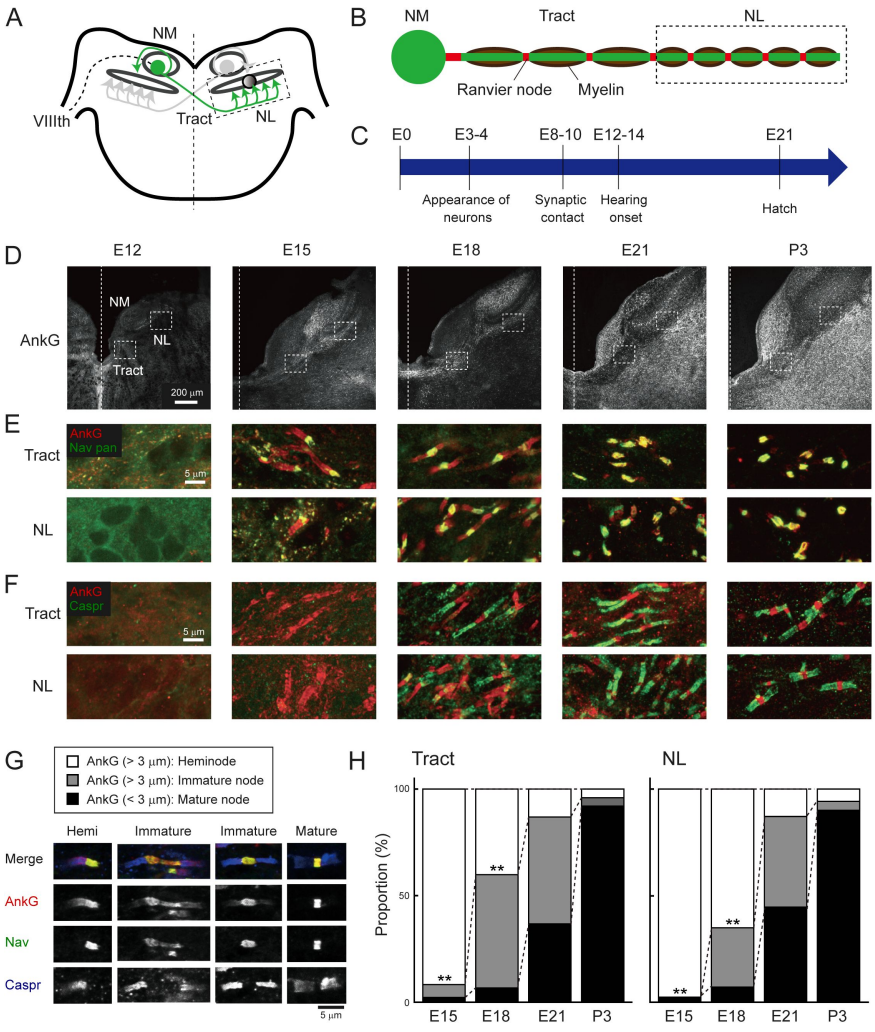

Figure 1.

Development of Ranvier nodes progressed in a similar time course along NM axons after hearing onset.

(A) Axonal projection of NM neurons in the chicken brainstem. NM axon projects to both sides of NL and forms “delay line” at contralateral NL. VIIIth, auditory nerve.
(B) Regional bias in periodic spacing of Ranvier nodes along the main trunk of NM axon. Internodal length is long at midline tract region and becomes shorter at the NL region in the axon.
(C) Development of NM neurons. NM neurons make synaptic contact with NL neurons by E10 and receive synaptic input from the auditory nerve by E12.
(D) Immunostaining of AnkG between E12 and P3. Dashed line indicates midline.
(E–F) Double immunostaining of AnkG (red) and panNav (green) for (E), and AnkG (red) and Caspr (green) for (F) at tract (upper) and NL (lower) regions from the same slices.
(G–H) Ranvier nodes matured on a similar time course across the region. Three types of Ranvier nodes immunostained with AnkG (red), panNav (green), and Caspr (blue) antibodies. (G), and their proportions between E15 and P3 (H). These types were determined according to the length of AnkG signals; the signals longer than 3 μm were defined as heminode or immature node according to the number of Nav-negative paranodal domains, and those shorter than 3 μm were defined as mature node. Note that some immature nodes had long nodal domains that exceeded 5 μm. This may correspond to a gap between the two heminodes. E15: n=183 and 177 nodes for tract and NL, N=4 chicks; E18: n=344 and 267 nodes for tract and NL, N=4 chicks; E21: n=267 and 371 nodes for tract and NL, N=4 chicks; P3: n=226 and 412 nodes for tract and NL, N=3 chicks. Statistical analysis: Chi-square test (H) was used to compare the proportions of node types between the regions at each developmental stage. **$p < 0.01$.

In this study, we tested the potential factors contributing to the regional differences in the nodal spacing along NM axons using high-resolution 3D morphometry of the optically-cleared brainstem auditory circuit. The results showed that NM axons are almost fully myelinated by oligodendrocytes with distinct morphological features after hearing onset. This morphological difference was not due to axonal structure. Inhibition of vesicular release from NM axons did not affect the internodal length and oligodendrocyte morphology but caused unmyelinated segments on NM axons via a suppression of oligodendrogenesis at the NL region. These results identified that the major factor contributing to the biased nodal spacing pattern in the ITD circuit is the regional heterogeneity in the intrinsic properties of oligodendrocytes. Activity-dependent signaling also contributed to this circuit by ensuring the density of oligodendrocytes through enhanced oligodendrogenesis. Our findings provide new insights into the mechanism of regulating nodal spacing along single axons and also into the significance of oligodendrocyte heterogeneity in neural circuit function.

Results

Ranvier nodes developed in a similar time course along NM axons after hearing onset

NM neurons in chick embryos form axonal projections to the NL at embryonic day 10 (E10), begin to receive auditory input from around E12, and are functionally mature by the time around hatch (Akter et al., 2018; 2020) (**Figure 1C**), allowing the animals to localize sounds immediately after hatching (Grier et al., 1967). To clarify how node formation progresses along development and whether there are regional differences in the timing of node formation, we examined the development of nodes at the tract and NL regions by double staining with AnkG and pan Nav antibodies or AnkG and Caspr antibodies, a marker for the paranodal domain (**Figure 1D–F**).

At E12, we did not find these molecules at each region. At E15, Nav-positive clusters appeared and they were localized specifically at one end of the fibrous AnkG signals. The remaining Nav-negative part of AnkG signals would correspond to the paranodal domain, as myelin sheath at the domain shows transient expression of AnkG during the immature period of CNS (Chang et al., 2014), and these structures were defined as 'heminode'. At E18, Caspr signals became detectable at the paranodal domain of heminode. In addition, some Caspr signals appeared on both sides of the fibrous AnkG signals, sandwiching the Nav cluster. These structures would be formed through the fusion of adjacent heminodes and were defined as 'immature node'. At E21, many nodes showed mature patterns, with complete colocalization of Nav and AnkG at a short nodal domain, which was flanked by Caspr-positive paranodal domains ('mature node'). Triple staining of these molecules confirmed the three stages of nodal development along the axon of NM neurons. Quantification of their abundance revealed that their maturation progressed gradually after hearing onset and was almost completed around hatch. 90 % of the node types were heminodes at E15. This decreased to about 50% by E18 and to about 10% by E21 (**Figure 1G, H**), suggesting that NM axons are almost fully myelinated by E21. Although the increase in the proportion of immature nodes was slightly preceded at the tract region, the overall tendency did not differ greatly between the regions. These data indicate that the formation of Ranvier nodes progress in a similar time course along the axon.

Development of myelin sheath along NM axons

Formation of Ranvier nodes requires maturation of myelin sheaths. To clarify their relationship on NM axons, we also examined the development of myelin with an antibody against myelin associated glycoprotein (MAG) during the period of node formation.

The immunosignals for MAG appeared around the midline of the brainstem at E12 and extended along the axons of NM neurons at E15, becoming more intense at later ages for both tract and NL regions (**Figure 2A, B**). These are consistent with the time course of node formation. Importantly, many oligodendrocytes were situated along the axon, as identified by immunopositivity of Olig2, a marker in the nucleus of oligodendrocyte lineage cells (**Figure 2C**). In addition, the MAG signals overlapped with the heminodes at E15. (**Figure 2D**), indicating that myelin sheaths already exist around the paranodal domains at the very early stage of node formation, in agreement with the idea that the early nodes can shift their position dynamically with myelin maturation (**Figure 2E**). These raised the questions as to when the biased nodal spacing pattern emerges during development and whether and how oligodendrocytes contribute to the process.

Internodal length was determined roughly during node formation

To answer these questions, we first evaluated the internodal length between mature/immature nodes at E18 and P9 at the tract and NL regions. These two time points correspond to the periods during and after node formation, respectively. We labeled axons with a tracer, rhodamine dextran, visualized nodes with the Caspr antibody, and measured the internodal length at each region (**Figure 2F**).

The internodal length was about 3 times longer in the tract region compared with the NL region at P9 (tract: 211.1±9.6 μm; NL: 63.9±3.0 μm) (**Figure 2G**), as observed in posthatch animals (Seidl et al., 2010). The difference in internodal length in these two regions of the axons was already evident at E18, although the internodal length was shorter by 20% at E18 in both tract and NL regions (tract: 171.0±7.0 μm; NL: 53.4±3.8 μm). The slightly shorter internodal length at E18 would reflect an elongation of internode during development in accordance with maturation of the brain size. Thus, the nodal spacing pattern was already determined at the early period of node formation, implying that reorganization of internodes would not contribute to the biased internodal length.

Morphology of oligodendrocytes differed between tract and NL regions

We next explored the contributions of oligodendrocytes to the regional difference in internodal length by evaluating the morphology of individual oligodendrocytes at E21. We sparsely labeled mature oligodendrocytes by expressing tdTomato with a palmitoylation signal (paltdTomato) under MBP promoter using *in ovo* electroporation and the iOn switch (Kumamoto et al., 2020) (**Figure 3A, B**), while labeling bilateral NM axons with GFP by transfection of avian adeno-associated virus (A3V) (**Figure 3C**). The 3D morphology of oligodendrocytes was then observed in 200 μm-thick brainstem slices optically cleared with SlowFade Glass mountant (**Figure 3D**) (Video 1, 2). We focused our analyses on oligodendrocytes ensheathing the main trunk of NM axons.

As presumed, length of myelin sheaths differed significantly between the tract and NL regions (tract: 174.1±5.0 μm; NL: 59.7±2.4 μm) (**Figure 3E**), which was consistent with the difference in internodal length between the regions (**Figure 2B**). Importantly, the diameter of myelin sheath including the axon did not differ between the regions and did not show any correlation with the myelin length (tract: 1.69±0.05 μm; NL: 1.64±0.07 μm) (**Figure 3F, G**). In each oligodendrocyte, the average myelin length was shorter by 3 times (tract: 181.1±7.3 μm NL: 63.6±4.7 μm), the number of myelin sheaths was larger by 2 times (tract: 3.0±0.2; NL: 6.6±0.6), and the total myelin length was shorter by 1.3 times (tract: 527.9±27.2 μm; NL: 394.6±29.7 μm) at the NL region compared to the tract region (**Figure 3H–J**). In addition, the cell body size was 30% smaller in cross-sectional area at the NL region (tract: 78.2±2.7 μm^2; NL: 52.5±1.9 μm^2) (**Figure 3K**). Thus,

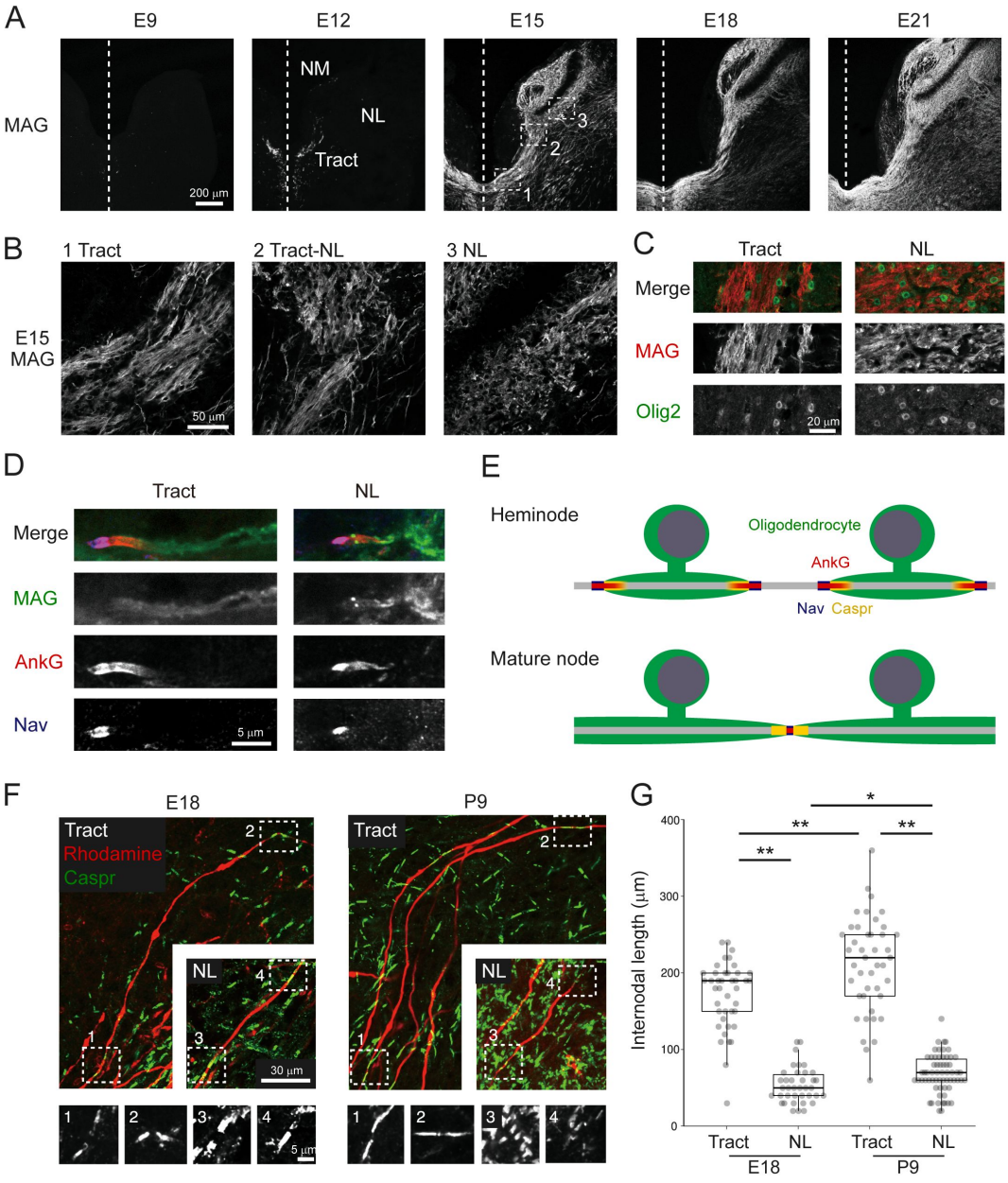

Figure 2.

Regional difference in internodal length was evident during development.

(A–B) Immunostaining of MAG between E9 and E21 (A). Boxes with numbers at E15 are magnified (B).
(C) Double immunostaining of MAG (red) and Olig2 (green), a marker of oligodendrocyte lineage cells, at E15.
(D) Localization of MAG (green), AnkG (red), and Nav (blue) on heminode at E15.
(E) Ranvier node is formed by restricting a gap between adjacent two heminodes during development. Note that paranodal domains, flanking the Nav-positive nodal domain, accompany fibrous AnkG clustering in heminode but not in mature node.
(F–G) Regional difference in internodal length appeared during the period of node formation. The axons were labeled with rhodamine dextran (red) and stained with Caspr antibody (green) at E18 and P9 (F). Internodal length was measured as a distance between adjacent mature/immature nodes (G). Boxes with numbers correspond to high-magnification images of each node. E18: n=41 internodes, N=4 chicks for tract, n=38 internodes, N=11 chicks for NL; P9: n=43 internodes, N=7 chicks for tract, n=62 internodes, N=10 chicks for NL.
Statistical analysis: Kruskal-Wallis test and post hoc Steel-Dwass test (G) was used to compare different developmental stages in the same region and different regions at the same developmental stage: *p < 0.05, **p < 0.01.

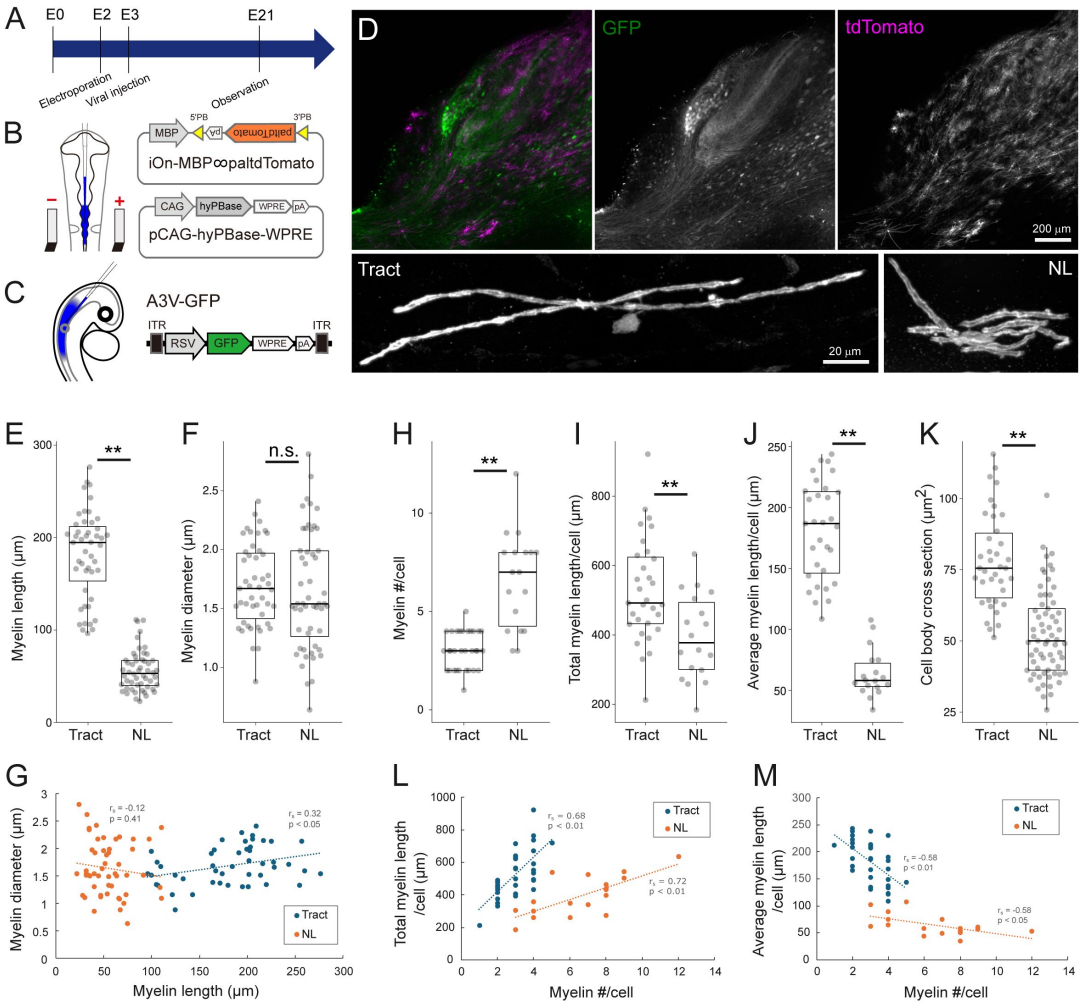

Figure 3.

3D morphometry of oligodendrocytes showed distinct differences between tract and NL regions.

(A) Timeline of experiments. *In ovo* electroporation and A3V transfection were performed at E2 (HH stage 11–12) and E2–3 (HH stage 15–16), respectively, and brainstem was observed at E21.
(B) Two types of plasmid vectors were introduced to visualize mature oligodendrocytes using *in ovo* electroporation. iOn-MBP∞paltdTomato expresses tdTomato with a palmitoylation signal (paltdTomato) under the control of the MBP promoter after the genomic integration. pCAG-hyPBase integrates the above plasmid into the genome by expressing hyperactive piggyBac transposase.
(C) A3V-GFP was injected into neural tube to visualize the axon of NM neurons.
(D) GFP and paltdTomato expressions in a 200-μm-thick slice (upper) and magnified images of single oligodendrocytes at tract and NL regions (lower). NM neurons and their axons were densely labeled with GFP (green), while mature oligodendrocytes were sparsely labeled with paltdTomato (magenta). **(E–G)** Myelin morphometry showed concordance with internodal length and their uncorrelation with myelin diameter. Length (E) and diameter (F) of myelin sheaths were compared between regions, and their relationship (G) was evaluated with Spearman's rank correlation coefficient (r_s). These parameters did not correlate with each other at both regions. Tract: n=47 myelins, N=3 chicks; NL: n=52 myelins, N=3 chicks.
(H–M) Oligodendrocyte morphometry highlighted their regional heterogeneity. Number (H), total length (I), average length of myelin sheaths (J) per oligodendrocyte, and cross-sectional area of cell body **(**K) were compared between regions. The relationship between total (L) or average (M) myelin lengths and the number of myelin sheaths was evaluated with Spearman's rank correlation coefficient (r_s). Total and average myelin lengths showed increasing and decreasing tendencies, respectively, with an increase of myelin processes. H, I, J, L, M: n=31 cells, N=4 chicks for tract, n=18 cells, N=3 chicks for NL. K: n=38 cells, N=3 chicks for tract, n=65 cells, N=3 chicks for NL.
Statistical analysis: Wilcoxon rank sum test (E, H, J, K), two-tailed Welch's t-test (F), and two-tailed Student's t-test (I): *p < 0.05, **p < 0.01, n.s., not significant.

oligodendrocyte morphology was heterogeneous, with distinct differences in several aspects between the tract and NL regions (**Figure 3L, M**), even though they were myelinating the same axons.

Axon structure did not contribute to the regional difference in nodal spacing

The distinct oligodendrocyte morphologies imply differences in their intrinsic properties (e.g., the ability to produce and extend myelin sheaths), but the involvement of other external constraints cannot yet be ruled out. The structure of axons, such as branch points and diameter, is one of these external constraints, and can affect myelin extension (Murray & Blakemore, 1980; Hildebrand et al., 1983; Ibrahim et al., 1995; Bechler et al., 2015; Stedehouder et al., 2019). We therefore investigated the relationship between the structural features of NM axons and the nodal spacing at E21. To accomplish this, we labeled the axon of NM neurons by expressing GFP with a palmitoylation signal (palGFP) using *in ovo* electroporation and examined the nodal spacing three-dimensionally along the main trunk of NM axon in 200 μm-thick brainstem slices, which were optically cleared after staining with a Caspr antibody (**Figure 4A–D**) (Video 3).

The results showed that on the main trunk of the axons, most of the Caspr signals showed mature/immature node patterns, confirming that the axons were almost fully myelinated. These axons formed multiple collateral branches innervating the ventral dendritic layer at the NL region, and triads of paranodal domains were frequently observed at the branch points. The internodal length (73.1±2.1 μm) was about 40% shorter compared to the branch point interval (122.5±6.7 μm) at the NL region (**Figure 4E, F**). Correspondingly, the number of internodes between adjacent branch points averaged 1.6 and was correlated with the length of branch point interval (‘0’: 27.5±3.9 μm; ‘1’: 79.3±5.1 μm; ‘2’: 156.3±7.1 μm; ‘3≦’: 232.0±10.0 μm) (**Figure 4H, I**). In areas with very short branch point intervals (bottom 10%: <40 μm), the axon lacked Caspr signals frequently (61.5%), implying that these areas are less likely to be myelinated (internode=0 μm) (**Figure 4G**). On the other hand, even in areas with long branch point intervals (top 10%: >220 μm), the internodal length did not increase and it was 2 times shorter than that at the tract region (<220 μm: 71.4±2.4 μm; >220 μm: 79.9±3.9 μm; tract: 164.3±4.2 μm) (**Figure 4J**). These observations suggest that the branch point interval is not a critical determinant of the short internodes at the NL region, although it can be a limiting factor in areas with the shorter branch point interval.

The diameter of axon main trunk did not differ between the tract and NL regions (tract: 1.40±0.03 μm; NL: 1.47±0.04 μm) (**Figure 4K**), corresponding to the diameter of myelin sheaths including axon (**Figure 3F**). This was consistent with the previous report showing that the axon diameter did not differ between the tract and the distal portion of ventral NL, at which the axon main trunk is situated (Seidl et al., 2010), confirming that the diameter of NM axons is not a factor determining the regional differences in nodal spacing.

Oligodendrogenesis was augmented at NL region

Given that NM axons were fully myelinated, oligodendrocyte density could also be a constraint of individual oligodendrocyte morphology; if the density is high, it may limit the extension of myelin sheath due to mutual competition for territory on the axon. Therefore, we examined the density of oligodendrocyte lineage cells during development by labeling the cells with the Olig2 antibody and quantifying their density at the tract and NL regions between E9 and E21(**Figure 5A** top, B).

The results showed that the density of Olig2-positive cells increased with development, peaked at E15, and decreased slightly afterwards. Importantly, the extent of this increase was more robust and about 1.3-fold higher at the NL region than at the tract region. The differences in oligodendrocyte density could result from several factors, including the density of oligodendrocyte precursor cells (OPCs), which mature into oligodendrocytes through several steps of maturation,

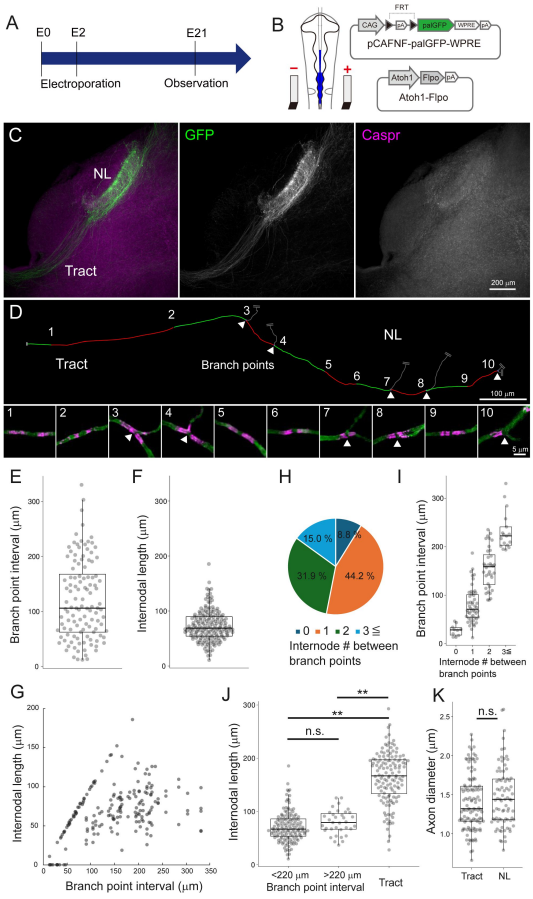

Figure 4.

Axonal structure was not a major determinant of regional difference in nodal spacing.

(A) Timeline of experiments. *In ovo* electroporation was performed at E2 (HH Stage 11–12), and brainstem was observed at E21.

(B) Two types of plasmid vectors were introduced to visualize the axon of NM neurons using *in ovo* electroporation. Atoh1-Flpo expresses Flpo under the control of Atoh1 promoter, which has selectivity for NM neurons. pCAFNF-palGFP-WPRE expresses GFP with a palmitoylation signal (palGFP) in a Flpo-dependent manner.

(C) Contralateral projections of NM neurons were labeled with palGFP (green), while visualizing paranodes with Caspr antibody (magenta) in a 200-μm-thick slice.

(D) Nodal spacing across tract and NL regions along a single NM axon. Arrowheads indicate branch points of collaterals. Each number corresponds to high-magnification images of node (lower panels). Each internode (between nodes) on the axon was labeled alternately with red and green lines, and their lengths were measured.

(E–G) Internodal length was clearly shorter than the branch point interval at the NL region. Branch point interval (E) at the NL region, internodal length (F) within those intervals, and their relationship (G). Note that the internodal length was mostly below 100 μm at the NL region even when the branch point interval was above 100 μm. E: n=113 intervals, F: n=178 internodes, G: n=188 internodes (including 0 μm), N=6 chicks.

(H–I) Branch point interval correlated with the number of internodes within the interval. Number of internodes between adjacent branch points (H) and branch point interval against the number of internodes (I). “0”: n=10 intervals; “1”: n=50 intervals; “2”: n=36 intervals; “3≦”: n=17 intervals.

(J) Internodal length was not necessarily specified by branch point interval. Comparison of internodal length for branch point intervals above 220 μm (top 10% of measured values), below 220 μm at the NL region, and at the tract region. <220: n=143 internodes, >220: n=35 internodes; Tract: n=132 internodes, N=5 chicks.

(K) Diameter of main trunk of the axon at tract and NL regions was not different. Tract: n=114 axons, N=3 chicks; NL: n=81 axons, N=3 chicks.

Statistical analysis: Kruskal-Wallis test and post hoc Steel-Dwass test (J) and Wilcoxon rank sum test (K): *p < 0.05, **p < 0.01, n.s., not significant.

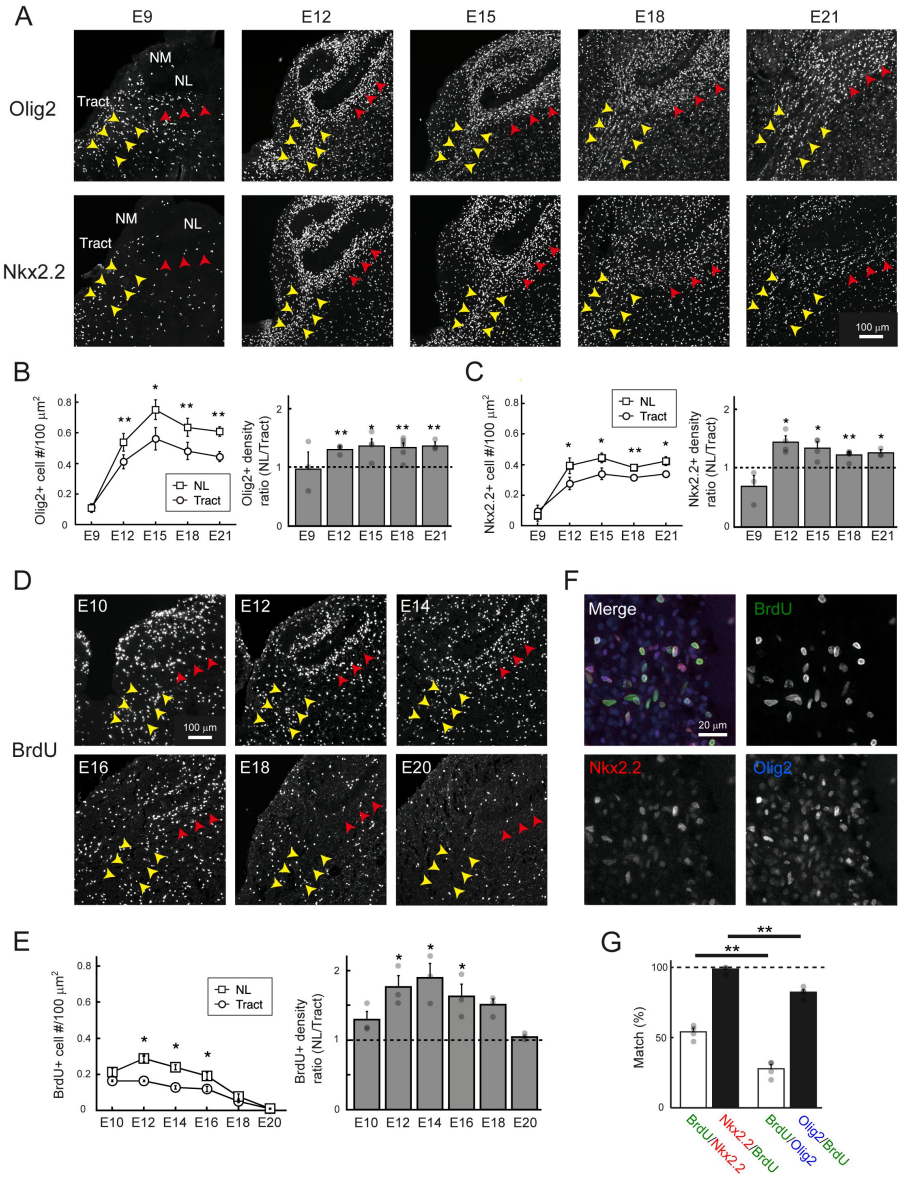

Figure 5.

Region-specific facilitation of oligodendrogenesis led to higher oligodendrocyte density at NL region.

(A) Immunostainings of Olig2, a marker for oligodendrocyte lineage cells, and Nkx2.2, a marker for OPCs. Yellow and red arrowheads indicate tract and NL regions, respectively.
(B–C) Density of developing oligodendrocytes increased especially at the NL region. Developmental changes in the density of Olig2-positive (B) and Nkx2.2-positive (C) cells at each region and their ratio between the regions. E9: N=3 chicks, E12: N=4 chicks, E15: N=4 chicks, E18: N=6 chicks, E21: N=3 chicks.
(D) Immunostaining of BrdU, a marker for proliferating cells. Yellow and red arrowheads indicate tract and NL regions, respectively.
(E) Cell proliferation was facilitated at the NL region. Developmental changes in the density of BrdU-positive cells at each region and their ratio between the regions. N=3 chicks for each stage.
(F) Colocalization of BrdU (green), Nkx2.2 (red), and Olig2 (blue) signals at E12.
(G) Proliferating cells were almost exclusively OPCs. Mutual percentages between BrdU-positive cells and Nkx2.2-or Olig2-positive cells at E12 and E14. N=4 chicks.
Statistical analysis: Two-tailed paired t-test (B, C, E), Wilcoxon rank sum test (G): *p < 0.05, **p < 0.01.

as well as the migration, proliferation, and differentiation of these cells. We measured the density of OPCs by labeling the cells with Nkx2.2 antibodies (**Figure 5A** bottom, C) (Xu et al., 2000). The density of Nkx2.2-positive cells increased sharply and reached a plateau by E12 at both regions, while the extent of this increase was also higher at the NL region. These cells were restricted to the ventral and dorsal fiber layers and almost absent in the somatic and dendritic layers of NL. These results suggest that the density of OPCs increases around the period of hearing onset to a larger extent at the NL region, contributing to the higher density of oligodendrocyte lineage cells at this region. We evaluated the level of proliferation of OPCs with BrdU labeling and found that the density of BrdU-positive cells was significantly higher at the NL region during E12–16 (**Figure 5D, E**). BrdU-positive cells were immunopositive for both Olig2 and Nkx2.2, confirming that they were OPCs (**Figure 5F, G**). These results suggest that the higher densities of OPCs and oligodendrocyte lineage cells at the NL region occur through a region-specific facilitation of oligodendrogenesis.

Inhibition of vesicular release did not affect internodal length but caused unmyelinated segments at NL region

Myelination could be modulated adaptively by neuronal activity (Fields, 2015; Bechler et al., 2018; Bonetto et al., 2021; Osanai et al., 2022). We here tested the possible contributions of activity-dependent adaptive mechanisms to the nodal spacing at E21 by using enhanced tetanus neurotoxin light chains (eTeNT), a genetically encoded silencing tool inhibiting vesicular release from axons (Kinoshita et al., 2012; Sooksawate et al., 2013). Using A3V, we expressed GFP-tagged eTeNT in most of the bilateral NM neurons (89.7±1.6%, N=6 chicks) and compared their effects on nodal spacing along these axons between the regions (**Figure 6A–D**).

The results showed that although Caspr-positive nodes were still observed in the axons expressing eTeNT, these axons exhibited a ~30% increase in the fraction of heminodes specifically at the NL region (A3V-GFP: 12.4%; A3V-eTeNT: 41.1%), resulting in the emergence of unmyelinated segments (A3V-GFP: 4.6±1.2%; A3V-eTeNT: 17.6±3.0%) (**Figure 6D–G**). Interestingly, eTeNT expression did not affect the internodal length at both tract and NL regions (**Figure 6H**). The internodal lengths at the NL region did not differ between those with (65.4±2.6 μm) and without (71.7±2.3 μm) heminodes, while the length of unmyelinated segments was only less than half of them (30.7±2.4 μm) (**Figure 6I**). Notably, the increase in the fraction of heminodes and the emergence of unmyelinated segments at the NL region did not occur when the same eTeNT construct was sparsely expressed by *in ovo* electroporation (heminodes: 14.7%; unmyelinated segments: 2.5 ± 1.2%) (Figure 6—figure supplement 1). These results indicate that the inhibition of vesicular release from most NM axons leads to a reduction in the density of myelin sheaths, with little effect on their length, thereby causing unmyelinated segments at the NL region.

Inhibition of vesicular release did not affect oligodendrocyte morphology but suppressed oligodendrogenesis at NL region

The reduction of myelin sheath density by A3V-eTeNT could occur through a decrease in the number of myelin sheaths formed by each oligodendrocyte and/or through a decrease in the density of oligodendrocytes themselves. To test these possibilities, we sparsely labeled mature oligodendrocytes, while transfecting A3V-eTeNT into bilateral NM neurons, and evaluated the effects of eTeNT on their morphology at E21 (**Figure 6J, K**).

The results showed that eTeNT affected neither the number nor the length of myelin sheaths in each oligodendrocyte at the NL region, supporting the conclusion that the oligodendrocyte morphology is determined in region-specific but activity-independent manners along NM axons.

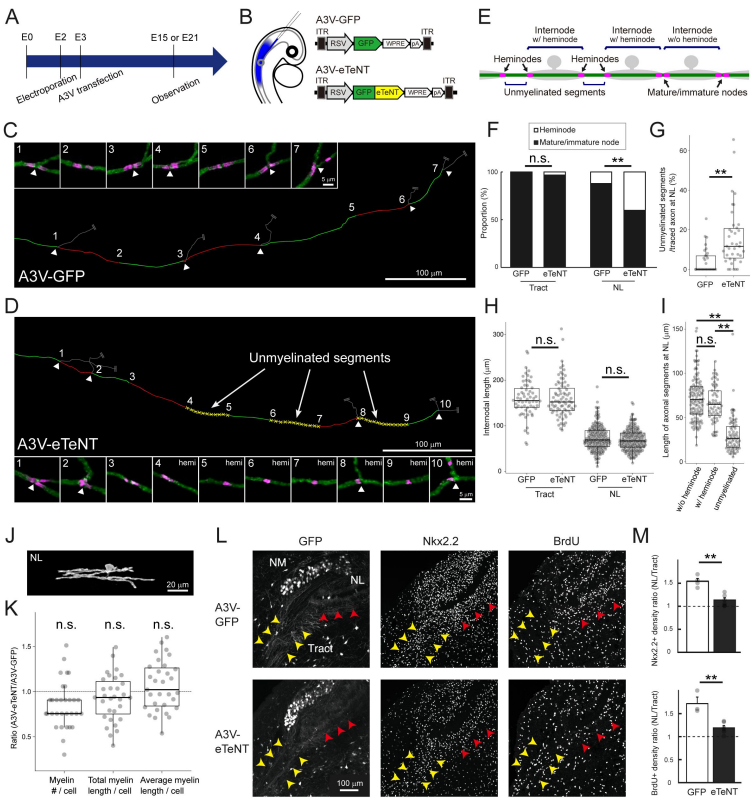

Figure 6.

Inhibition of vesicular release caused unmyelinated segments via suppression of oligodendrogenesis at NL region.

(A) Timeline of experiments. *In ovo* electroporation and A3V transfection were performed at E2 (HH Stage 11–12) and at E2–3 (HH Stage 15–16), respectively, and brainstem was observed at E15 in (L– M) and at E21 in (C–K).
(B) A3V-eTeNT expressing GFP-tagged eTeNT was used to inhibit vesicular release from NM axons. A3V-GFP expressing only GFP was used as a control
(C–I) eTeNT caused unmyelinated segments at the NL region without affecting internodal length. Most of the axons were labeled with A3V-GFP (C) or A3V-eTeNT (D), while nodal spacing was analyzed along one of the axons. Arrowheads indicate branch points of collaterals. Each number corresponds to high-magnification images of the node. Each internode was labeled alternately with red and green lines, while unmyelinated segments were labeled with yellow broken lines for A3V-eTeNT. “Unmyelinated segment” was identified as a non-overlapping axonal segment formed by a pair of heminodes, while internodes were classified into “internode w/o heminode” and “internode w/ heminode” according to the types of nodes at the ends (E) (see Methods). Percentages of heminode and mature/immature node (F), and internodal length (H) at tract and NL regions. Percentage of unmyelinated segments in each axon traced over 200 μm (G), and length of each segment including internode w/o and w/ heminode, and unmyelinated segment for A3V-eTeNT (I) at the NL region. F: GFP (n=124 nodes) and eTeNT (n=160 nodes) at tract, GFP (n=186 nodes) and eTeNT (n=270 nodes) at NL. G: n=29 axons for GFP, n=38 axons for eTeNT. H: GFP (n=62 internodes) and eTeNT (n=80 internodes) at tract, GFP (n=178 internodes) and eTeNT (n=180 internodes) at NL. I: Internode w/o (n=115) and w/ (n=63) heminode and unmyelinated segment (n=63). Tract: N=3 chicks for GFP, N=4 chicks for eTeNT, NL: N=5 chicks for GFP, N=5 chicks for eTeNT.
(J–K) eTeNT did not affect oligodendrocyte morphology at the NL region. Magnified images of single oligodendrocytes after A3V-eTeNT transfection (J). Number, total length, average length of myelins per oligodendrocyte were compared between A3V-eTeNT and A3V-GFP (**Figure 4** H–J) and shown as a ratio (K; n=31 cells, N=4 chicks).
(L–M) eTeNT suppressed oligodendrogenesis at the NL region. Immunostainings of Nkx2.2 (OPC marker) and BrdU (proliferating cell marker) at E15 for A3V-GFP (upper) and A3V-eTeNT (lower)
(L). Yellow and red arrowheads indicate tract and NL regions, respectively. Relative density of Nkx2.2- and BrdU-positive cells between the tract and NL regions (M). A3V-eTeNT reduced the density of these cells specifically at the NL region and abolished the difference between the regions. M: N=4 chicks for GFP, N=6 chicks for eTeNT.
Statistical analysis: Chi-square test (F), Wilcoxon rank sum test (G, H, K), Kruskal-Wallis test and post hoc Steel-Dwass test (I) and two-tailed student’s t-test (M): *p < 0.05, **p < 0.01, n.s., not significant.

To determine if inhibiting vesicular release from axons alters proliferation of OPCs, we examined the density of Nkx2.2-positive OPCs and BrdU-positive proliferating cells at E15 in the A3V-eTeNT and control (A3V-GFP) conditions (**Figure 6L, M**). In the control group, the density of these cells became higher by 1.5 folds at the NL region compared to the tract region (see also **Figure 5C, E**). In the eTeNT group, on the other hand, this enhancement was suppressed, which abolished the difference in the density of these cells between the regions. These data indicate that vesicular release from NM axons promotes oligodendrogenesis specifically at the NL region without altering oligodendrocyte morphology, suggesting that adaptive oligodendrogenesis is important in covering the entire length of the axon with short myelin sheaths at the region (**Figure 7A–C**).

Discussion

This study identified several factors responsible for biased nodal spacing patterns along axons, including heterogeneity in oligodendrocyte morphology, regional differences in proliferation of OPCs, and activity-dependent signaling from axons through vesicular release.

Using the chick brainstem auditory circuit known for its characteristic nodal spacing as a model, we found that NM axons were almost fully myelinated by oligodendrocytes with distinct morphologies between the two regions having markedly different internodal lengths. This regional heterogeneity reflected differences in the intrinsic property of oligodendrocytes in these two regions rather than the extrinsic constraints. Expression of eTeNT in most of the NM axons caused unmyelinated segments by region-specific suppression of oligodendrogenesis without affecting internodal length or oligodendrocyte morphology, suggesting that primary role of neural activity is to ensure the oligodendrocyte density necessary for full myelination of axons.

Biased nodal spacing pattern reflects regional heterogeneity of oligodendrocyte

The major factor contributing to regional differences in internodal length along NM axons was regional heterogeneity in oligodendrocyte morphology. The morphological differences were observed not only in the length of myelin sheaths, but also in the number of myelin sheaths and the size of cell bodies (**Figure 3**). Considering the morphological classification of oligodendrocytes by Pío del Río-Hortega (1928), oligodendrocytes at the tract and NL regions could be classified into type III and type II, respectively. Such morphological heterogeneity could be related to the variation of gene profiles among oligodendrocytes (Butt et al., 1998; Marques et al., 2016; Osanai et al., 2022; Valihrach et al., 2022). Differences in the origin and/or the pericellular microenvironment of OPCs during development may contribute to the diverse gene profiles of oligodendrocytes (Crawford et al., 2016; Foerster et al., 2019, 2024; Boshans et al., 2020; Sherafat et al., 2021). Consistent with the idea, OPCs in the brainstem have two developmental origins, derived from the ventral and dorsal sides of the hindbrain (Vallstedt et al., 2005). In addition, pericellular concentration of some ligands may differ between the tract and NL regions according to the distance from synapses or postsynaptic cells. Whether the gene profiles of oligodendrocytes and OPCs differ between the tract and NL regions and what causes the differences are important issues to be examined in the future.

The regional differences in the morphology of oligodendrocytes would primarily reflect their intrinsic properties specific to each region; the ability of myelin production is higher, while that of myelin extension is lower at the NL region than at the tract region. Supportively, the axonal factors, such as structure and vesicular release, did not affect the regional heterogeneity in oligodendrocyte morphology (**Figure 4**, **6H**). Oligodendrocyte density did not affect the morphology, either; the number and length of myelin sheaths did not increase even when unmyelinated segments appeared after A3V-eTeNT transfection (**Figure 6J–K**). Another potential factor influencing the regional differences in internodal length could be pre-nodal clusters which

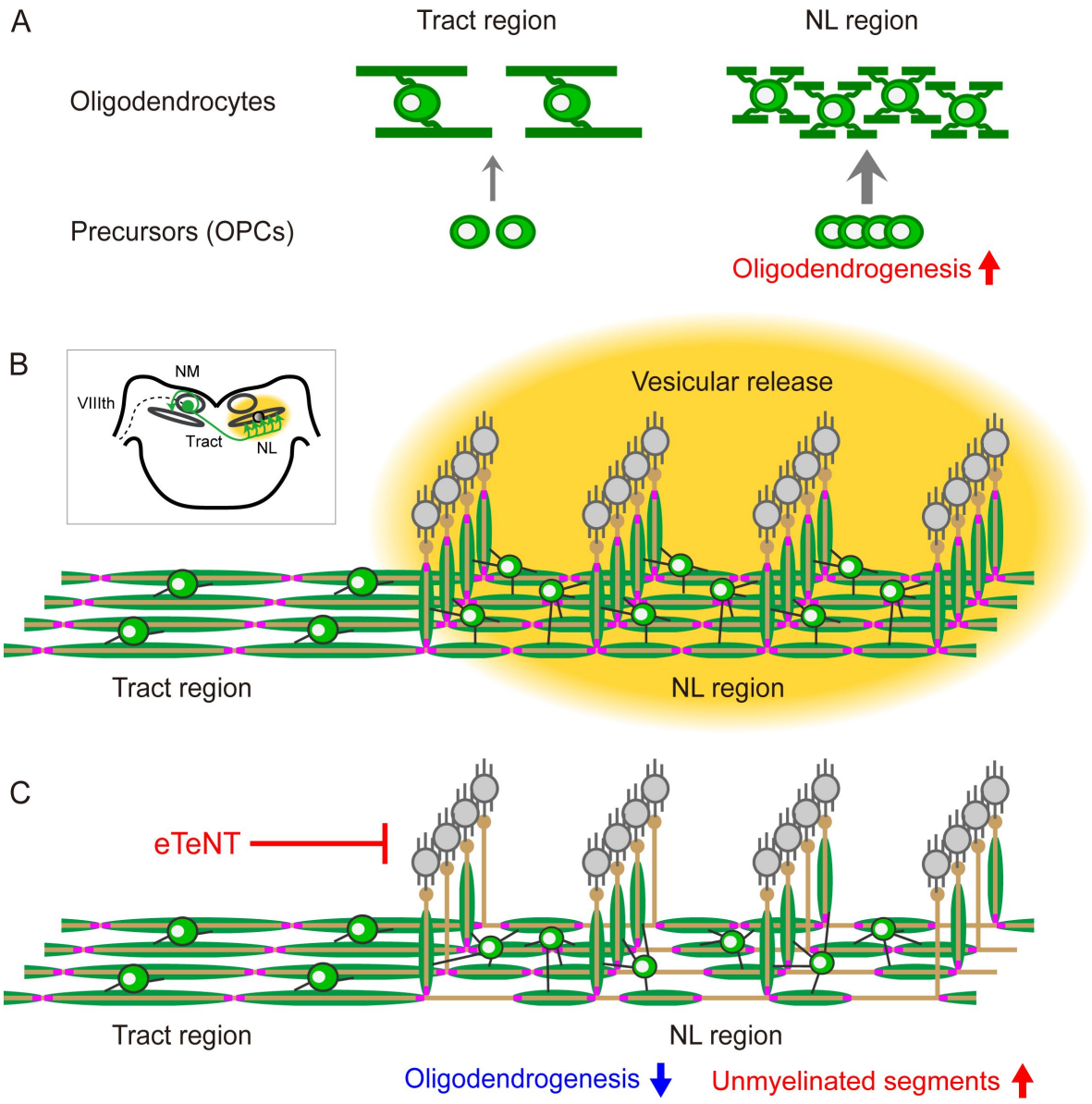

Figure 7.

Regional heterogeneity of oligodendrocytes and adaptive oligodendrogenesis underlie the biased nodal spacing pattern along NM axons.

(A) Morphology of oligodendrocytes, such as the number and length of myelins, is determined intrinsically at each region; those at the NL region have larger numbers of short myelins compared to those at the tract region. In addition, adaptive oligodendrogenesis increases the density of oligodendrocytes specifically at the NL region.
(B–C) Nodal spacing primarily reflects the length of myelins at each region (B). Inhibition of vesicular release from NM axons by eTeNT suppressed adaptive oligodendrogenesis and caused unmyelinated segments at the NL region without altering oligodendrocyte morphology and internodal length (C), suggesting the importance of adaptive oligodendrogenesis in myelinating the entire axons with the short myelins at the NL region. Thus, intrinsic and adaptive properties of oligodendrocytes play a pivotal role in shaping the region-specific nodal spacing along NM axons.

are formed by cell-autonomous accumulation of nodal components on the axons of certain types of neurons before myelination (Kaplan et al., 1997; Freeman et al., 2015; Vagionitis et al., 2022). However, our immunostaining results failed to detect such clusters on the NM axons. This may be due to limited detection sensitivity or the unavailability of neurofascin antibodies in chickens. Nevertheless, it is unlikely that fixed pre-nodal clusters pre-determine internodal length prior to myelination, given the facts that the length of unmyelinated segments was far shorter than the internodal length at the NL region (**Figure 6I**). Thus, we consider that the morphology of oligodendrocyte, and hence the length of myelin sheaths, are determined according to the intrinsic properties of oligodendrocytes at each region, which underlies the regional differentiation of nodal spacing along NM axons. Variations in the intrinsic properties of oligodendrocytes are also reported in other brain regions. Oligodendrocytes in white matter are morphologically distinct from those in gray matter, and their original features did not change even when OPCs were cross-transplanted (Viganò et al., 2013). In addition, OPCs collected from different brain regions show their original morphological features when cultured on artificial fibers (Bechler et al., 2015). In summary, our findings provide the perspective that oligodendrocytes with different intrinsic properties work together to fine-tune the neural circuit function involved in ITD detection.

Adaptive oligodendrogenesis ensures full myelination of axons at NL region

Neuronal activity can affect the proliferation, maturation and morphology of oligodendrocytes, but the effects are not uniform across different neuronal subtypes and brain regions (Gibson et al., 2014; Yang et al., 2020; Bonetto et al., 2021; Osanai et al., 2022). Indeed, the inhibition of vesicular release had different effects on myelination depending on neuronal subtype; myelination is impaired in some axons, but remains unaffected in others (Mensch et al., 2015; Koudelka et al., 2016). In NM axons, activity-dependent signaling did not affect myelin formation in mature oligodendrocytes but instead facilitated proliferation and differentiation of OPCs. Given that this enhancement of oligodendrogenesis occurred specifically at the NL region (**Figure 5**, **6I**) and that unmyelinated segments were increased only when eTeNT was expressed in a large fraction of the axons via A3V (**Figure 6F–G**, Figure 6—figure supplement 1), exocytosis from the presynaptic terminals of NM axons would cause the effects by altering the perisynaptic microenvironment. Glutamate and several trophic factors such as BDNF, which are released from the terminals of NM axons, may act on the OPC directly via spillover from the synapse and/or indirectly via activation of NL neurons or astrocytes (Du et al., 2003; Pease-Raissi & Chan, 2021; Fekete & Nishiyama, 2022; Pivoňková et al., 2024). Supportively, mRNA of NR1, a major subunit of NMDA receptor, is strongly expressed in glial cells, presumably oligodendrocyte lineage cells, at the ventral and dorsal dendritic layers of NL after E10 (Tang and Carr, 2007). Future studies are needed to determine what ligands mediate the differentiation and proliferation of OPCs as the activity-dependent signaling at the NL region and whether there are regional differences in the sensitivity of these OPCs to the ligands along the NM axon.

Adaptive oligodendrogenesis would support the function of brainstem auditory circuits by ensuring the full myelination of NM axons. Full myelination of the auditory pathway enables rapid membrane responses and high metabolic support during high-frequency firing, which are critical for precise and reliable processing of sound information (Kim et al., 2013; Moore et al., 2020). Moreover, the full myelination at the NL region, which is mediated by the adaptive enhancement of oligodendrogenesis, would be particularly important for ITD detection. The contralateral projections of NM neurons have a sequential branching structure called a “delay line” at the ventral area of NL in chickens. This delay line produces an output delay of up to 180 μs for contralateral NL neurons along the medial to lateral axis (Overholt et al., 1992). This delay covers the physiological ITD range for the chicken, allowing the ITDs to be encoded in a “place map” within the NL (Jeffress, 1948; Köppl & Carr, 2008). This should provide the neural basis for the ability of excellent sound localization in chickens, which can discriminate ITDs of about 20

μs (8.9° minimum audible angle) (Krumm et al., 2022). Reliable myelination of the delay line ensures constant conduction velocity and output delay and hence is critical for precise ITD calculation. Thus, the adaptive oligodendrogenesis at the NL region would be a mechanism that secures the accuracy of ITD calculation in the avian auditory circuit. Interestingly, ITD representation within the NL exhibits plasticity around the period of hearing onset in the barn owl (Carr et al., 2024), which coincides with the period of adaptive oligodendrogenesis, speculating its contribution to the plasticity.

Commonalities and differences with the sound localization circuit in mammals

Regional regulation of conduction velocity has also been reported in mammals. In a brainstem auditory circuit of gerbils, which is involved in the processing of ITDs, several regional differentiations have been observed in the nodal spacing along the axon. In the axon of spherical bushy cells, a mammalian homologue of NM neurons, the internodal length is longer for contralateral side than for ipsilateral side, presumably compensating for the different axonal pathlength between the two sides (Seidl & Rubel, 2016). On the other hand, in the axon of globular bushy cells that project to medial nucleus of trapezoid body, the internodal length is longer for those innervating more medial location (i.e. more distal location), ensuring simultaneous inputs within the nucleus (Ford et al., 2015). These regional differentiations of nodal spacing would be acquired independently in mammals and birds through evolutionary convergence (Lipovsek & Wingate, 2018), emphasizing their importance in securing ITD computation in the microsecond order. Notably, in globular bushy cells, neural activity did not alter the nodal spacing, but instead regulated the conduction velocity by adaptively changing the axon diameter (Nabel et al., 2024), suggesting that the mechanism of action of activity-dependent signaling is different among neurons and species. It will be interesting to examine whether regional heterogeneity in the intrinsic properties of oligodendrocytes is a prominent determinant in the biased nodal spacing pattern in mammalian ITD circuits as well. Such comparisons will help to understand the fundamental logic and mechanisms of determining nodal spacing patterns along the axons.

Conclusion

This study identified the factors mediating the regional differentiation of nodal spacing along single axons in the auditory pathway of chicken; the differentiation of nodal spacing reflects regional heterogeneity in oligodendrocyte morphology, and the activity-dependent signaling from axons via vesicular release contributes to the full myelination of axons through region-specific enhancement of oligodendrogenesis. The results in this model system provide evidence that oligodendrocyte heterogeneity, which is widely observed in the brain, can contributes to achieving optimal timing of signals and optimal function of local circuits in the nervous system.

Materials and methods

Animals

Chickens (*Gallus domesticus*) of either sex between embryonic day 9 (E9) and posthatch day 9 (P9) were used for experiments. The care of experimental animals was in accordance with the regulations on animal experiments at Nagoya University and the experiments were approved by the institutional committee. Fertilized eggs were incubated in a humidified incubator at 37.5°C to desired stage. The developmental stage of embryos was determined according to the Hamburger and Hamilton (1951) series. Chicks were deeply anesthetized with Isoflurane (FUJIFILM Wako, Japan), and embryos were anesthetized by cooling eggs in ice-cold water. Brainstem tissues containing middle-one third of NM were mostly used for experiments (Kuba et al., 2005).

Immunohistochemistry

Mouse pan Nav antibody (5 µg/ml, Sigma), rabbit AnkG antibody (5 µg/ml, a gift from Gisèle Alcaraz, Bouzidi et al., 2002), mouse Caspr antibody (2 µg/ml, NeuroMab), mouse MAG antibody (2 µg/ml, Merck), rabbit Olig2 antibody (2 µg/ml, a gift from Hirohide Takebayashi, Takebayashi et al., 2000), mouse Nkx2.2 antibody (2 µg/ml, DSHB), rat BrdU antibody (10 µg/ml, Abcam), rabbit GFP antibody (2 µg/ml, MBL), rat GFP antibody (2 µg/ml, Santa Cruz), rabbit RFP antibody (2 µg/ml, Rockland) were used for immunohistochemistry. Chicks were perfused transcardially with a periodate-lysine-paraformaldehyde fixative (ml/g body weight): 1% (w/v) paraformaldehyde, 2.7% (w/v) lysine HCl, 0.21% (w/v) $NaIO_4$, and 0.1% (w/v) Na_2HPO_4. The brainstem was postfixed for 1.5 hours at 4 °C. After cryoprotection with 30% (w/w) sucrose in PBS, coronal sections (20–30 µm) were obtained. The sections were incubated overnight with the primary antibodies, then with Alexa-conjugated secondary antibodies (10 µg/ml, Molecular Probes) for 2 hours and were observed under a confocal laser-scanning microscope (FV1000, Olympus). For each image, 6-9 confocal planes were Z-stacked with a step of 0.8 µm. Images were analyzed in Fiji (Schindelin et al., 2012).

Anterograde labeling of NM axons was made by injecting dextran (MW 3000) conjugated with TMR (Life Technologies, 10–40% in 0.1 M phosphate buffer adjusted to pH 2.0 with HCl) into the midline tract region through a patch pipette and incubating the brainstem in the HG-ACSF for 30 min at 38 °C (Lawrence and Trussell, 2000; Wirth et al., 2008).

Internodal length was measured as follows. Images were captured with a ×60, 1.35-NA objective (Olympus), and 6-10 confocal planes were Z-stacked with maximum projection. Internodal length was defined as a distance between adjacent nodes, which was determined by identifying a pair of Caspr signals. Number of oligodendrocytes and their precursors was measured as follows. Images were captured with a ×20, 0.75-NA objective (Olympus), and a single confocal plane was used for the measurement. The number was measured automatically by setting a threshold in areas over 14000 μm^2 at each region.

BrdU labeling

BudU (10 mg/ml in PBS, Nacalai, Japan) was injected subcutaneously into embryos (0.1 mg/g body weight) one hour before fixation, and sections were prepared as described above. The sections were mounted on a cover slide, treated with 2M HCl for 40 min at 60 °C, and used for immunohistochemistry.

Plasmids

Following plasmids were used for *in ovo* electroporation: iOn-MBP∞paltdTomato, pCAG-hyPBase, pCAFNF-palGFP-WPRE and Atoh1-Flpo (a gift from Marcela Lipovsek, Lipovsek & Wingate, 2018). All plasmids were constructed by inserting the following sequences into the plasmid backbones of iOn-CAG∞MCS (Addgene #154013, Kumamoto et al., 2020), pCAG-EGFP-WPRE and pCAG-floxedSTOP-tdTomato-WPRE (Egawa and Yawo, 2019) using In-Fusion® Snap Assembly Master Mix (Takara) or NEBuilder® HiFi DNA Assembly Master Mix (NEB); 1.9 kb sequence of mouse MBP promoter (a gift from Yasuyuki Osanai), hyPBase (pCMV-hyPBase, a gift from Wellcome Trust Sanger Institute; Yusa et al., 2011), CAFNF sequence (pCAFNF-GFP, addgene #13772; Matsuda et al., 2007), palGFP (pAAV2 SynTetOff-palGFP, a gift from Hiroyuki Hioki; Sohn et al., 2017). For A3V production, pA3V-RSV-EGFP and pA3V-RSV-EGFP.eTeNT were used. The latter was also used for *in ovo* electroporation in Figure 6—figure supplement 1. pA3V-RSV-EGFP.eTeNT was constructed by inserting eTeNT sequence (HiRet-TRE-EGFP.eTeNT; Kinoshita et al., 2012) into the plasmid backbones of pA3V-RSV-EGFP (Matsui et al., 2012). All constructs were verified by Sanger sequencing.

In ovo electroporation

Plasmids were introduced into chick embryos in the same manner as previously reported (Jahan et al., 2023). Briefly, plasmid cocktail (0.4–0.5 μg/μl of each) was injected into the neural tube of chick embryos at E2 (HH Stage 10–12; Hamburger and Hamilton, 1951) and introduced into the right side of the hindbrain (rhombomere 3–8). The electrical pulses were applied using a pair of electrodes (CUY613P1, NEPAGENE) placed in parallel at 2 mm apart. The settings of electroporator (NEPA21, NEPAGENE) were as follows; poring pulse: 15 V, 30 ms width, 50 ms interval, 3 pulses, 10% decay and transfer pulse: 5 V, 50 ms width, 50 ms interval, 5 pulses, 40% decay.

A3V transfection

A3V-GFP and A3V-eTeNT were prepared as previously reported (Matsui et al., 2012). Their yield was approximately 10^{13} genome copies (GC)/mL. Viral solution containing 0.05% Fast Green (Nakarai tesque) was injected into the lumen of neural tube near the ear vesicle at E2–3 (60–70 hours of incubation, HH stage 15–16), at which A3V infects NM neurons with high efficiency (Matsui et al., 2012).

Immunostaining and 3D-imaging of 200 μm-thick brainstem slices

Chick embryos were perfused transcardially at E21 with PBS containing 10 U/mL heparin followed by 4% (w/v) paraformaldehyde in PBS. The brainstem was postfixed overnight at 4 °C. After cryoprotection with 30% (w/w) sucrose in PBS, coronal sections (200 μm thickness) were obtained. The brainstem slices were delipidated and permeabilized with cold acetone for 3 min, washed in PBS containing 0.1% (w/v) NaBH4 for 5 min to remove autofluorescence, and stained with primary antibody for 3 days, followed by secondary antibody for 1 day. The stained slices were embedded with SlowFade Glass Soft-set Antifade Mountant (Thermo Fisher Scientific) using 200 μm-thick silicone rubber spacer and No.0 coverslip (CG00C2, ThorLab), thereby making them transparent.

3D images were captured with a ×60, 1.42-NA oil-immersion objective (UPLXAPO60XO, Olympus) or ×100, 1.5-NA oil-immersion objective (UPLAPO100XOHR, Olympus) under a spinning disk confocal laser-scanning microscope (SpinSR10, Olympus). For each image, approximately 600 confocal planes were Z-stacked with a step of 0.3 μm. Multiple 3D images were stitched together using Imaris Stitcher (Oxford Instruments).

3D morphometry

In the 3D images captured by SpinSR10, myelin length, internode length, and branch point interval were traced using SNT (Arshadi et al., 2021), a Fiji plugin. Oligodendrocytes presumed not myelinating NM axons (e.g., oligodendrocytes that are not present within NM axon bundles or whose myelin sheaths barely along the axon bundle) were excluded from the analysis. For myelin and axon diameters, the length between intensity peaks of membrane-localized fluorescent proteins on a line orthogonal to the axon was measured. For nodal spacing along a single axon, three different axonal segments were defined according to the types of nodes at the ends; “internode w/o heminode” was a segment between mature/immature nodes, “internode w/ heminode” was a segment either between a mature/immature node and a heminode, or between heminodes flanking unmyelinated segments when the axon was separated by multiple heminodes, and “unmyelinated segment” was a non-overlapping segment between heminodes consisting of adjacent internodes. Quantified data were graphed using PlotsOfData (Postma et al., 2019) or Excel (Microsoft).

Statistics

Statistical analysis was performed using R software (*http://cran.r-project.org/*). Data normality was assessed using the Shapiro-Wilk test. Non-normally distributed data were analyzed using non-parametric tests: the Wilcoxon rank sum test for comparisons between two groups (**Figures 3E**, **3H**, **3J**, **3K**, **4K**, **5G**, **6G**, **6H**, **6K**), and the Kruskal-Wallis test with post hoc Steel-Dwass test for comparisons among more than two groups (**Figures 2G**, **4J**, **6I**). Normally distributed data were evaluated for equality of variance by Levene's test; two-tailed Student's t-test (**Figures 3I**, **6M**) was used for equal variance, and two-tailed Welch's t-test (**Figure 3F**) for unequal variance. Two-tailed paired t-test was used for comparisons of paired data between two groups measured from the same brainstem slice (**Figures 5B**, **5C**, **5E**). Chi-squared test was used to compare the proportions between groups (**Figures 1H**, **6F**). Correlations were assessed using Spearman's rank correlation coefficient (**Figures 3G**, **3L**, **3M**). The significance level was set at 0.05. Data are presented as mean ± standard error of the mean (SEM).

Acknowledgements

Special thanks to R. Douglas Fields and Sian Lewis for their insightful feedback and suggestions on this manuscript. We acknowledge Division for Medical Research Engineering, Nagoya University Graduate School of Medicine for usage of SpinSR10, Imaris Stitcher and NanoDrop 2000. We thank Gisèle Alcaraz and Hirohide Takebayashi for kindly distributing AnkyrinG and Olig2 antibodies. We also thank Kazuhiro Nakamura and Chika Nishimura for cooperation in A3V production. Further thanks are extended to Connie Cepko, Jean Livet, Marcela Lipovsek, Hiroyuki Hioki, Yasuyuki Osanai and Wellcome Trust Sanger Institute for a gift of pCAFNF-GFP (Addgene #13772; Matsuda et al., 2007), iOn-CAG∞MCS (Addgene #154013; Kumamoto et al., 2020), Atoh1-Flpo (Lipovsek & Wingate, 2018), pAAV2 SynTetOff-palGFP, 1.9-kb MBP promoter, and pCMV-hyPBase (Yusa et al., 2011) respectively. This work was supported by Grants-in-aid from MEXT KAKENHI (19H04747, 21H02577, 22K19358 and 24H00584 to HK; 17K07039, 20K15915 and 23K05986 to RE) and the Takeda Science Foundation to HK.

Additional information

Author contributions

RE, HK designed the work.

RE, HK performed histochemistry.

RE, KH traced internode length.

RE made plasmid vectors, performed electroporation and 3D analysis

RM, DW made the A3V vectors.

RE, HK wrote the paper.

All authors edited the manuscript, read and approved the final manuscript.

Funding

Japan Science and Technology Agency (JST) (19H04747)

Japan Science and Technology Agency (JST) (21H02577)

Japan Science and Technology Agency (JST) (22K19358)

Japan Science and Technology Agency (JST) (24H00584)

Japan Science and Technology Agency (JST) (20K15915)

Japan Science and Technology Agency (JST) (23K05986)

Additional files

Video 1. *High-resolution 3D serial images of oligodendrocytes at the tract region of a 200-μm-thick brainstem slice. NM axons were densely labeled with GFP (green) and mature oligodendrocytes (magenta) were sparsely labeled with paltdTomato. The three z-stack images were stitched together. Field of view: 614.89×222.08×180.9 μm.*

Video 2. *High-resolution 3D serial images of oligodendrocytes at the NL region of a 200-μm-thick brainstem slice. NM axons were densely labeled with GFP (green) and mature oligodendrocytes (magenta) were sparsely labeled with paltdTomato. The three z-stack images were stitched together. Field of view: 626.58×222.08×184.5 μm.*

Video 3. *High-resolution 3D serial images of nodal spacing pattern along NM axon at the tract and NL regions of a 200-μm-thick brainstem slice. NM axons were labeled with GFP (green), and Caspr (magenta) was immunostained. The six z-stack images were stitched together. Field of view: 1237.35×217.97×185.4 μm.*

Supplemental Data 1. *Sparse expression of eTeNT did not cause unmyelinated segments.* ***(A)*** *Timeline of experiments. In ovo electroporation was performed at E2 (HH Stage 11–12), and the brainstem was analyzed at E21.* ***(B)*** *The plasmid vector originally used to generate A3V-eTeNT was electroporated into the right side of the hindbrain.* ***(C–E)*** *Node formation was not affected in axons with sparse eTeNT expression. Contralateral projections of NM neurons were sparsely labeled with GFP-tagged eTeNT (green), and paranodes were visualized with Caspr immunostaining (magenta) in 200-μm-thick brainstem slices (C). The percentages of heminodes and mature/immature nodes (D), as well as the percentage of unmyelinated segments per traced axon at the NL region (E), were comparable to those shown in Figure 6F–G for A3V-GFP-transfected axons. D: n=102 nodes at tract, n=129 nodes at NL. E: n=26 axons. N=4 chicks. Statistical analysis: Chi-square test (D), Wilcoxon rank sum test (E): *p < 0.05, **p < 0.01, n.s., not significant.*

References

Akter N., Adachi R., Kato A., Fukaya R., Kuba H (2018) **Auditory Input Shapes Tonotopic Differentiation of Kv1.1 Expression in Avian Cochlear Nucleus during Late Development** *The Journal of neuroscience: the official journal of the Society for Neuroscience* **38**:2967–2980 https://doi.org/10.1523/JNEUROSCI.2472-17.2018 | Google Scholar

Akter N., Fukaya R., Adachi R., Kawabe H., Kuba H (2020) **Structural and Functional Refinement of the Axon Initial Segment in Avian Cochlear Nucleus during Development** *The Journal of neuroscience: the official journal of the Society for Neuroscience* **40**:6709–6721 https://doi.org/10.1523/JNEUROSCI.3068-19.2020 | Google Scholar

Arshadi C., Günther U., Eddison M., Harrington K. I. S., Ferreira T. A (2021) **SNT: a unifying toolbox for quantification of neuronal anatomy** *Nature methods* **18**:374–377 https://doi.org/10.1038/s41592-021-01105-7 | Google Scholar

Bechler M. E., Byrne L., Ffrench-Constant C (2015) **CNS Myelin Sheath Lengths Are an Intrinsic Property of Oligodendrocytes** *Current biology: CB* **25**:2411–2416 https://doi.org/10.1016/j.cub.2015.07.056 | Google Scholar

Bechler M. E., Swire M., Ffrench-Constant C (2018) **Intrinsic and adaptive myelination-A sequential mechanism for smart wiring in the brain** *Developmental neurobiology* **78**:68–79 https://doi.org/10.1002/dneu.22518 | Google Scholar

Bonetto G., Belin D., Káradóttir R. T (2021) **Myelin: A gatekeeper of activity-dependent circuit plasticity?** *Science* **374**:eaba6905 https://doi.org/10.1126/science.aba6905 | Google Scholar

Boshans L. L., Sherafat A., Nishiyama A (2020) **The effects of developmental and current niches on oligodendrocyte precursor dynamics and fate** *Neuroscience letters* **715**:134593 https://doi.org/10.1016/j.neulet.2019.134593 | Google Scholar

Bouzidi M., Tricaud N., Giraud P., Kordeli E., Caillol G., Deleuze C., Couraud F., Alcaraz G (2002) **Interaction of the Nav1.2a subunit of the voltage-dependent sodium channel with nodal ankyrinG. In vitro mapping of the interacting domains and association in synaptosomes** *The Journal of biological chemistry* **277**:28996–29004 https://doi.org/10.1074/jbc.M201760200 | Google Scholar

Butt A. M., Ibrahim M., Gregson N., Berry M (1998) **Differential expression of the L- and S-isoforms of myelin associated glycoprotein (MAG) in oligodendrocyte unit phenotypes in the adult rat anterior medullary velum** *Journal of neurocytology* **27**:271–280 https://doi.org/10.1023/a:1006996713413 | Google Scholar

Carr C. E., Konishi M (1990) **A circuit for detection of interaural time differences in the brain stem of the barn owl** *The Journal of neuroscience: the official journal of the Society for Neuroscience* **10**:3227–3246 https://doi.org/10.1523/JNEUROSCI.10-10-03227.1990 | Google Scholar

Carr C. E., Wang T., Kraemer I., Capshaw G., Ashida G., Köppl C., Kempter R., Kuokkanen P. T (2024) **Experience-Dependent Plasticity in Nucleus Laminaris of the Barn Owl** *The Journal*

of neuroscience: the official journal of the Society for Neuroscience **44**:e0940232023 https://doi.org/10.1523/JNEUROSCI.0940-23.2023 | Google Scholar

Chang K. J., Zollinger D. R., Susuki K., Sherman D. L., Makara M. A., Brophy P. J., Cooper E. C., Bennett V., Mohler P. J., Rasband M. N (2014) **Glial ankyrins facilitate paranodal axoglial junction assembly** *Nature neuroscience* **17**:1673–1681 https://doi.org/10.1038/nn.3858 | Google Scholar

Chong S. Y., Rosenberg S. S., Fancy S. P., Zhao C., Shen Y. A., Hahn A. T., McGee A. W., Xu X., Zheng B., Zhang L. I., Rowitch D. H., Franklin R. J., Lu Q. R., Chan J. R (2012) **Neurite outgrowth inhibitor Nogo-A establishes spatial segregation and extent of oligodendrocyte myelination** *Proceedings of the National Academy of Sciences of the United States of America* **109**:1299–1304 https://doi.org/10.1073/pnas.1113540109 | Google Scholar

Crawford A. H., Tripathi R. B., Richardson W. D., Franklin R. J. M (2016) **Developmental Origin of Oligodendrocyte Lineage Cells Determines Response to Demyelination and Susceptibility to Age-Associated Functional Decline** *Cell reports* **15**:761–773 https://doi.org/10.1016/j.celrep.2016.03.069 | Google Scholar

Del Río Hortega P. (1928) **Tercera aportación al conocimiento morfológico e interpretación functional de la oligodendroglia** *Mem. Real Soc. Esp. Hist. Nat* **14**:5–122 Google Scholar

Du Y., Fischer T. Z., Lee L. N., Lercher L. D., Dreyfus C. F (2003) **Regionally specific effects of BDNF on oligodendrocytes** *Developmental neuroscience* **25**:116–126 https://doi.org/10.1159/000072261 | Google Scholar

Egawa R., Yawo H (2019) **Analysis of Neuro-Neuronal Synapses Using Embryonic Chick Ciliary Ganglion via Single-Axon Tracing, Electrophysiology, and Optogenetic Techniques** *Current protocols in neuroscience* **87**:e64 https://doi.org/10.1002/cpns.64 | Google Scholar

Fekete C. D., Nishiyama A (2022) **Presentation and integration of multiple signals that modulate oligodendrocyte lineage progression and myelination** *Frontiers in cellular neuroscience* **16**:1041853 https://doi.org/10.3389/fncel.2022.1041853 | Google Scholar

Fields R. D (2015) **A new mechanism of nervous system plasticity: activity-dependent myelination** *Nature reviews Neuroscience* **16**:756–767 https://doi.org/10.1038/nrn4023 | Google Scholar

Foerster S., Hill M. F. E., Franklin R. J. M (2019) **Diversity in the oligodendrocyte lineage: Plasticity or heterogeneity?** *Glia* **67**:1797–1805 https://doi.org/10.1002/glia.23607 | Google Scholar

Foerster S., Floriddia E. M., van Bruggen D., Kukanja P., Hervé B., Cheng S., Kim E., Phillips B. U., Heath C. J., Tripathi R. B., Call C., Bartels T., Ridley K., Neumann B., López-Cruz L., Crawford A. H., Lynch C. J., Serrano M., Saksida L., Rowitch D. H., ..., Franklin R. J. M. (2024) **Developmental origin of oligodendrocytes determines their function in the adult brain** *Nature neuroscience* **27**:1545–1554 https://doi.org/10.1038/s41593-024-01666-8 | Google Scholar

Ford M. C., Alexandrova O., Cossell L., Stange-Marten A., Sinclair J., Kopp-Scheinpflug C., Pecka M., Attwell D., Grothe B (2015) **Tuning of Ranvier node and internode properties in myelinated axons to adjust action potential timing** *Nature communications* **6**:8073 https://doi.org/10.1038/ncomms9073 | Google Scholar

Freeman S. A., Desmazières A., Simonnet J., Gatta M., Pfeiffer F., Aigrot M. S., Rappeneau Q., Guerreiro S., Michel P. P., Yanagawa Y., Barbin G., Brophy P. J., Fricker D., Lubetzki C., Sol-Foulon N (2015) **Acceleration of conduction velocity linked to clustering of nodal components precedes myelination** *Proceedings of the National Academy of Sciences of the United States of America* **112**:E321–E328 https://doi.org/10.1073/pnas.1419099112 | Google Scholar

Gibson E. M., Purger D., Mount C. W., Goldstein A. K., Lin G. L., Wood L. S., Inema I., Miller S. E., Bieri G., Zuchero J. B., Barres B. A., Woo P. J., Vogel H., Monje M (2014) **Neuronal activity promotes oligodendrogenesis and adaptive myelination in the mammalian brain** *Science* **344**:1252304 https://doi.org/10.1126/science.1252304 | Google Scholar

Grier J. B., Counter S. A., Shearer W. M (1967) **Prenatal auditory imprinting in chickens** *Science* **155**:1692–1693 https://doi.org/10.1126/science.155.3770.1692 | Google Scholar

Hamburger V., Hamilton H. L (1951) **A series of normal stages in the development of the chick embryo** *Journal of morphology* **88**:49–92 Google Scholar

Hildebrand C., Remahl S., Persson H., Bjartmar C (1993) **Myelinated nerve fibres in the CNS** *Progress in neurobiology* **40**:319–384 https://doi.org/10.1016/0301-0082(93)90015-k | Google Scholar

Hyson R. L (2005) **The analysis of interaural time differences in the chick brain stem** *Physiology & behavior* **86**:297–305 https://doi.org/10.1016/j.physbeh.2005.08.003 | Google Scholar

Ibrahim M., Butt A. M., Berry M (1995) **Relationship between myelin sheath diameter and internodal length in axons of the anterior medullary velum of the adult rat** *Journal of the neurological sciences* **133**:119–127 https://doi.org/10.1016/0022-510x(95)00174-z | Google Scholar

Jahan I., Adachi R., Egawa R., Nomura H., Kuba H (2023) **CDK5/p35-Dependent Microtubule Reorganization Contributes to Homeostatic Shortening of the Axon Initial Segment** *The Journal of neuroscience: the official journal of the Society for Neuroscience* **43**:359–372 https://doi.org/10.1523/JNEUROSCI.0917-22.2022 | Google Scholar

Jeffress L. A (1948) **A place theory of sound localization** *Journal of comparative and physiological psychology* **41**:35–39 https://doi.org/10.1037/h0061495 | Google Scholar

Kaplan M. R., Meyer-Franke A., Lambert S., Bennett V., Duncan I. D., Levinson S. R., Barres B. A (1997) **Induction of sodium channel clustering by oligodendrocytes** *Nature* **386**:724–728 https://doi.org/10.1038/386724a0 | Google Scholar

Kim J. H., Renden R., von Gersdorff H. (2013) **Dysmyelination of auditory afferent axons increases the jitter of action potential timing during high-frequency firing** *The Journal of neuroscience: the official journal of the Society for Neuroscience* **33**:9402–9407 https://doi.org/10.1523/JNEUROSCI.3389-12.2013 | Google Scholar

Kinoshita M., Matsui R., Kato S., Hasegawa T., Kasahara H., Isa K., Watakabe A., Yamamori T., Nishimura Y., Alstermark B., Watanabe D., Kobayashi K., Isa T (2012) **Genetic dissection of the circuit for hand dexterity in primates** *Nature* **487**:235–238 https://doi.org/10.1038/nature11206 | Google Scholar

Köppl C., Carr C. E (2008) **Maps of interaural time difference in the chicken's brainstem nucleus laminaris** *Biological cybernetics* **98**:541–559 https://doi.org/10.1007/s00422-008-0220-6 | Google Scholar

Koudelka S., Voas M. G., Almeida R. G., Baraban M., Soetaert J., Meyer M. P., Talbot W. S., Lyons D. A (2016) **Individual Neuronal Subtypes Exhibit Diversity in CNS Myelination Mediated by Synaptic Vesicle Release** *Current biology: CB* **26**:1447–1455 https://doi.org/10.1016/j.cub.2016.03.070 | Google Scholar

Krumm B., Klump G. M., Köppl C., Beutelmann R., Langemann U (2022) **Chickens have excellent sound localization ability** *The Journal of experimental biology* **225**:jeb243601 https://doi.org/10.1242/jeb.243601 | Google Scholar

Kuba H., Yamada R., Fukui I., Ohmori H (2005) **Tonotopic specialization of auditory coincidence detection in nucleus laminaris of the chick** *The Journal of neuroscience: the official journal of the Society for Neuroscience* **25**:1924–1934 https://doi.org/10.1523/JNEUROSCI.4428-04.2005 | Google Scholar

Kumamoto T., Maurinot F., Barry-Martinet R., Vaslin C., Vandormael-Pournin S., Le M., Lerat M., Niculescu D., Cohen-Tannoudji M., Rebsam A., Loulier K., Nedelec S., Tozer S., Livet J (2020) **Direct Readout of Neural Stem Cell Transgenesis with an Integration-Coupled Gene Expression Switch** *Neuron* **107**:617–630 https://doi.org/10.1016/j.neuron.2020.05.038 | Google Scholar

Lawrence J. J., Trussell L. O (2000) **Long-term specification of AMPA receptor properties after synapse formation** *The Journal of neuroscience: the official journal of the Society for Neuroscience* **20**:4864–4870 https://doi.org/10.1523/JNEUROSCI.20-13-04864.2000 | Google Scholar

Lipovsek M., Wingate R. J (2018) **Conserved and divergent development of brainstem vestibular and auditory nuclei** *eLife* **7**:e40232 https://doi.org/10.7554/eLife.40232 | Google Scholar

Marques S., Zeisel A., Codeluppi S., et al (2016) **Oligodendrocyte heterogeneity in the mouse juvenile and adult central nervous system** *Science* **352**:1326–1329 https://doi.org/10.1126/science.aaf6463 | Google Scholar

Matsuda T., Cepko C. L (2007) **Controlled expression of transgenes introduced by in vivo electroporation** *Proceedings of the National Academy of Sciences of the United States of America* **104**:1027–1032 https://doi.org/10.1073/pnas.0610155104 | Google Scholar

Matsui R., Tanabe Y., Watanabe D (2012) **Avian adeno-associated virus vector efficiently transduces neurons in the embryonic and post-embryonic chicken brain** *PloS one* **7**:e48730 https://doi.org/10.1371/journal.pone.0048730 | Google Scholar

Mensch S., Baraban M., Almeida R., Czopka T., Ausborn J., El Manira A., Lyons D. A (2015) **Synaptic vesicle release regulates myelin sheath number of individual oligodendrocytes in vivo** *Nature neuroscience* **18**:628–630 https://doi.org/10.1038/nn.3991 | Google Scholar

Moore S., Meschkat M., Ruhwedel T., Trevisiol A., Tzvetanova I. D., Battefeld A., Kusch K., Kole M. H. P., Strenzke N., Möbius W., de Hoz L., Nave K. A. (2020) **A role of oligodendrocytes in**

information processing *Nature communications* **11**:5497 https://doi.org/10.1038/s41467-020-19152-7 | Google Scholar

Murray J. A., Blakemore W. F (1980) **The relationship between internodal length and fibre diameter in the spinal cord of the cat** *Journal of the neurological sciences* **45**:29–41 https://doi.org/10.1016/s0022-510x(80)80004-9 | Google Scholar

Nabel A. L., Teich L., Wohlfrom H., Alexandrova O., Heß M., Pecka M., Grothe B (2024) **Development of myelination and axon diameter for fast and precise action potential conductance** *Glia* **72**:794–808 https://doi.org/10.1002/glia.24504 | Google Scholar

Normand E. A., Rasband M. N (2015) **Subcellular patterning: axonal domains with specialized structure and function** *Developmental cell* **32**:459–468 https://doi.org/10.1016/j.devcel.2015.01.017 | Google Scholar

Osanai Y., Yamazaki R., Shinohara Y., Ohno N (2022) **Heterogeneity and regulation of oligodendrocyte morphology** *Frontiers in cell and developmental biology* **10**:1030486 https://doi.org/10.3389/fcell.2022.1030486 | Google Scholar

Overholt E. M., Rubel E. W., Hyson R. L (1992) **A circuit for coding interaural time differences in the chick brainstem** *The Journal of neuroscience: the official journal of the Society for Neuroscience* **12**:1698–1708 https://doi.org/10.1523/JNEUROSCI.12-05-01698.1992 | Google Scholar

Pease-Raissi S. E., Chan J. R (2021) **Building a (w)rapport between neurons and oligodendroglia: Reciprocal interactions underlying adaptive myelination** *Neuron* **109**:1258–1273 https://doi.org/10.1016/j.neuron.2021.02.003 | Google Scholar

Pivoňková H., Sitnikov S., Kamen Y., Vanhaesebrouck A., Matthey M., Spitzer S. O., Ng Y. T., Tao C., de Faria O., Varga B. V., Káradóttir R. T. (2024) **Heterogeneity in oligodendrocyte precursor cell proliferation is dynamic and driven by passive bioelectrical properties** *Cell reports* **43**:114873 https://doi.org/10.1016/j.celrep.2024.114873 | Google Scholar

Postma M., Goedhart J (2019) **PlotsOfData-A web app for visualizing data together with their summaries** *PLoS biology* **17**:e3000202 https://doi.org/10.1371/journal.pbio.3000202 | Google Scholar

Rasband M. N., Peles E (2015) **The Nodes of Ranvier: Molecular Assembly and Maintenance** *Cold Spring Harbor perspectives in biology* **8**:a020495 https://doi.org/10.1101/cshperspect.a020495 | Google Scholar

Rasband M. N., Peles E (2021) **Mechanisms of node of Ranvier assembly** *Nature reviews Neuroscience* **22**:7–20 https://doi.org/10.1038/s41583-020-00406-8 | Google Scholar

Schindelin J., Arganda-Carreras I., Frise E., Kaynig V., Longair M., Pietzsch T., Preibisch S., Rueden C., Saalfeld S., Schmid B., Tinevez J. Y., White D. J., Hartenstein V., Eliceiri K., Stedehouder J., Brizee D., Slotman J. A., Pascual-Garcia M., Leyrer M. L., Bouwen B. L., Dirven C. M., Gao Z., Berson D. M., Houtsmuller A. B., Kushner S. A (2019) **Local axonal morphology guides the topography of interneuron myelination in mouse and human neocortex** *eLife* **8**:e48615 https://doi.org/10.7554/eLife.48615 | Google Scholar

Tomancak P., Cardona A (2012) **Fiji: an open-source platform for biological-image analysis** *Nature methods* **9**:676–682 https://doi.org/10.1038/nmeth.2019 | Google Scholar

Seidl A. H., Rubel E. W (2016) **Systematic and differential myelination of axon collaterals in the mammalian auditory brainstem** *Glia* **64**:487–494 https://doi.org/10.1002/glia.22941 | Google Scholar

Seidl A. H., Rubel E. W., Harris D. M (2010) **Mechanisms for adjusting interaural time differences to achieve binaural coincidence detection** *The Journal of neuroscience: the official journal of the Society for Neuroscience* **30**:70–80 https://doi.org/10.1523/JNEUROSCI.3464-09.2010 | Google Scholar

Seidl A. H., Rubel E. W., Barría A (2014) **Differential conduction velocity regulation in ipsilateral and contralateral collaterals innervating brainstem coincidence detector neurons** *The Journal of neuroscience: the official journal of the Society for Neuroscience* **34**:4914–4919 https://doi.org/10.1523/JNEUROSCI.5460-13.2014 | Google Scholar

Sherafat A., Pfeiffer F., Nishiyama A (2021) **Shaping of Regional Differences in Oligodendrocyte Dynamics by Regional Heterogeneity of the Pericellular Microenvironment** *Frontiers in cellular neuroscience* **15**:721376 https://doi.org/10.3389/fncel.2021.721376 | Google Scholar

Snaidero N., Möbius W., Czopka T., Hekking L. H., Mathisen C., Verkleij D., Goebbels S., Edgar J., Merkler D., Lyons D. A., Nave K. A., Simons M (2014) **Myelin membrane wrapping of CNS axons by PI(3,4,5)P3-dependent polarized growth at the inner tongue** *Cell* **156**:277–290 https://doi.org/10.1016/j.cell.2013.11.044 | Google Scholar

Sohn J., Takahashi M., Okamoto S., Ishida Y., Furuta T., Hioki H (2017) **A Single Vector Platform for High-Level Gene Transduction of Central Neurons: Adeno-Associated Virus Vector Equipped with the Tet-Off System** *PloS one* **12**:e0169611 https://doi.org/10.1371/journal.pone.0169611 | Google Scholar

Sooksawate T., Isa K., Matsui R., Kato S., Kinoshita M., Kobayashi K., Watanabe D., Kobayashi K., Isa T (2013) **Viral vector-mediated selective and reversible blockade of the pathway for visual orienting in mice** *Frontiers in neural circuits* **7**:162 https://doi.org/10.3389/fncir.2013.00162 | Google Scholar

Susuki K., Chang K. J., Zollinger D. R., Liu Y., Ogawa Y., Eshed-Eisenbach Y., Dours-Zimmermann M. T., Oses-Prieto J. A., Burlingame A. L., Seidenbecher C. I., Zimmermann D. R., Oohashi T., Peles E., Rasband M. N (2013) **Three mechanisms assemble central nervous system nodes of Ranvier** *Neuron* **78**:469–482 https://doi.org/10.1016/j.neuron.2013.03.005 | Google Scholar

Takebayashi H., Yoshida S., Sugimori M., Kosako H., Kominami R., Nakafuku M., Nabeshima Y (2000) **Dynamic expression of basic helix-loop-helix Olig family members: implication of Olig2 in neuron and oligodendrocyte differentiation and identification of a new member, Olig3** *Mechanisms of development* **99**:143–148 https://doi.org/10.1016/s0925-4773(00)00466-4 | Google Scholar

Tang Y. Z., Carr C. E (2007) **Development of N-methyl-D-aspartate receptor subunits in avian auditory brainstem** *The Journal of comparative neurology* **502**:400–413 https://doi.org/10.1002/cne.21303 | Google Scholar

Tomassy G. S., Berger D. R., Chen H. H., Kasthuri N., Hayworth K. J., Vercelli A., Seung H. S., Lichtman J. W., Arlotta P (2014) **Distinct profiles of myelin distribution along single axons of**

pyramidal neurons in the neocortex *Science* **344**:319–324 https://doi.org/10.1126/science.1249766 | Google Scholar

Vabnick I., Novaković S. D., Levinson S. R., Schachner M., Shrager P (1996) **The clustering of axonal sodium channels during development of the peripheral nervous system** *The Journal of neuroscience: the official journal of the Society for Neuroscience* **16**:4914–4922 https://doi.org/10.1523/JNEUROSCI.16-16-04914.1996 | Google Scholar

Vagionitis S., Auer F., Xiao Y., Almeida R. G., Lyons D. A., Czopka T (2022) **Clusters of neuronal neurofascin prefigure the position of a subset of nodes of Ranvier along individual central nervous system axons in vivo** *Cell reports* **38**:110366 https://doi.org/10.1016/j.celrep.2022.110366 | Google Scholar

Vallstedt A., Klos J. M., Ericson J (2005) **Multiple dorsoventral origins of oligodendrocyte generation in the spinal cord and hindbrain** *Neuron* **45**:55–67 https://doi.org/10.1016/j.neuron.2004.12.026 | Google Scholar

Valihrach L., Matusova Z., Zucha D., Klassen R., Benesova S., Abaffy P., Kubista M., Anderova M (2022) **Recent advances in deciphering oligodendrocyte heterogeneity with single-cell transcriptomics** *Frontiers in cellular neuroscience* **16**:1025012 https://doi.org/10.3389/fncel.2022.1025012 | Google Scholar

Viganò F., Möbius W., Götz M., Dimou L (2013) **Transplantation reveals regional differences in oligodendrocyte differentiation in the adult brain** *Nature neuroscience* **16**:1370–1372 https://doi.org/10.1038/nn.3503 | Google Scholar

Wirth M. J., Kuenzel T., Luksch H., Wagner H (2008) **Identification of auditory neurons by retrograde labelling for patch-clamp recordings in a mixed culture of chick brainstem** *Journal of neuroscience methods* **169**:55–64 https://doi.org/10.1016/j.jneumeth.2007.11.015 | Google Scholar

Xu X., Cai J., Fu H., Wu R., Qi Y., Modderman G., Liu R., Qiu M (2000) **Selective expression of Nkx-2.2 transcription factor in chicken oligodendrocyte progenitors and implications for the embryonic origin of oligodendrocytes** *Molecular and cellular neurosciences* **16**:740–753 https://doi.org/10.1006/mcne.2000.0916 | Google Scholar

Yang S. M., Michel K., Jokhi V., Nedivi E., Arlotta P (2020) **Neuron class-specific responses govern adaptive myelin remodeling in the neocortex** *Science* **370**:eabd2109 https://doi.org/10.1126/science.abd2109 | Google Scholar

Yusa K., Zhou L., Li M. A., Bradley A., Craig N. L (2011) **A hyperactive piggyBac transposase for mammalian applications** *Proceedings of the National Academy of Sciences of the United States of America* **108**:1531–1536 https://doi.org/10.1073/pnas.1008322108 | Google Scholar

Author information

Ryo Egawa
Department of Cell Physiology, Graduate School of Medicine, Nagoya University, Nagoya, Japan
ORCID iD: 0009-0009-8640-1529

Kota Hiraga
Department of Cell Physiology, Graduate School of Medicine, Nagoya University, Nagoya, Japan

Ryosuke Matsui
Department of Biological Sciences, Graduate School of Medicine, Kyoto University, Kyoto, Japan

Dai Watanabe
Department of Biological Sciences, Graduate School of Medicine, Kyoto University, Kyoto, Japan

Hiroshi Kuba
Department of Cell Physiology, Graduate School of Medicine, Nagoya University, Nagoya, Japan

For correspondence: kuba@med.nagoya-u.ac.jp

Editors

Reviewing Editor
Catherine Carr
University of Maryland, College Park, United States of America

Senior Editor
Sacha Nelson
Brandeis University, Waltham, United States of America

Reviewer #2 (Public review):

Summary:

Egawa et al describe the developmental timeline of the assembly of nodes of Ranvier in the chick brainstem auditory circuit. In this unique system, the spacing between nodes varies significantly in different regions of the same axon from early stages, which the authors suggest is critical for accurate sound localization. Egawa et al set out to determine which factors regulate this differential node spacing. They do this by using immunohistological analyses to test the correlation of node spacing with morphological properties of the axons, and properties of oligodendrocytes, glial cells that wrap axons with the myelin sheaths that flank the nodes of Ranvier. They find that axonal structure does not vary significantly, but that oligodendrocyte density and morphology varies in the different regions traversed by these axons, which suggests this is a key determinant of the region-specific differences in node density and myelin sheath length. They also find that differential oligodendrocyte density is partly determined by secreted neuronal signals, as (presumed) blockage of vesicle fusion with tetanus toxin reduced oligodendrocyte density in the region where it is normally higher. Based on these findings, the authors propose that oligodendrocyte morphology, myelin sheath length, and consequently nodal distribution are primarily determined by intrinsic oligodendrocyte properties rather than neuronal factors such as activity.

Major comments:

(1) The authors should test the efficiency of TeNT to validate that vesicular release is indeed inhibited from expressing neurons. Additionally, the authors should clarify if their TeNT

expression system results in the whole tract being silenced, or results in sparse vesicular release inhibition in only a few neurons.

(2) The authors should revise their statistical analyses throughout, and supply additional information to explain the rationale for the statistical tests used, including e.g. data normality, paired sampling, number of samples/independent biological replicates.

(3) The main finding of the study is that the density of nodes differs between two regions of the chicken auditory circuit, probably due to morphological differences in the respective oligodendrocytes. Can the authors discuss if this finding is likely to be specific to the avian auditory circuit?

(4) The study shows a correlation between node spacing and oligodendrocyte density, but the authors did not manipulate oligodendrocyte density per se (i.e. cell-autonomously). The authors should either include such experiments, or discuss their value in supporting the interpretation of their results.

(5) The authors should discuss very pertinent prior studies, in particular to contextualize their findings with (a) known neuron-autonomous modes of node formation prior to myelination, (b) known effects of vesicular fusion directly on myelinating capacity and oligodendrogenesis, (c) known correlation of myelin length and thickness with axonal diameter, (d) regional heterogeneity in the oligodendrocyte transcriptome.

Significance:

In our view the study tackles a fundamental question likely to be of interest to a specialized audience of cellular neuroscientists. This descriptive study is suggestive that in the studied system, oligodendrocyte density determines the spacing between nodes of Ranvier, but further manipulations of oligodendrocyte density per se are needed to test this convincingly.

https://doi.org/10.7554/eLife.106415.2.sa2

Reviewer #3 (Public review):

Summary:

The authors have investigated the myelination pattern along the axons of chick avian cochlear nucleus. It has already been shown that there are regional differences in the internodal length of axons in the nucleus magnocellularis. In the tract region across the midline, internodes are longer than in the nucleus laminaris region. Here the authors suggest that the difference in internodal length is attributed to heterogeneity of oligodendrocytes. In the tract region oligodendrocytes would contribute longer myelin internodes, while oligodendrocytes in the nucleus laminaris region would synthesize shorter myelin internodes. Not only length of myelin internodes differs, but also along the same axon unmyelinated areas between two internodes may vary. This is an interesting contribution since all these differences contribute to differential conduction velocity regulating ipsilateral and contralateral innervation of coincidence detector neurons. However, the demonstration falls rather short of being convincing.

Major comments:

(1) The authors neglect the possibility that nodal cluster may be formed prior to myelin deposition. They have investigated stages E12 (no nodal clusters) and E15 (nodal cluster plus MAG+ myelin). Fig. 1D is of dubious quality. It would be important to investigate stages between E12 and E15 to observe the formation of pre-nodes, i.e., clustering of nodal components prior to myelin deposition.

(2) The claim that axonal diameter is constant along the axonal length need to be demonstrated at the EM level. This would also allow to measure possible regional differences in the thickness of the myelin sheath and number of myelin wraps.

(3) The observation that internodal length differs is explain by heterogeneity of sources of oligodendrocyte is not convincing. Oligodendrocytes a priori from the same origin remyelinate shorter internode after a demyelination event.

Significance:

The authors suggest that the difference in internodal length is attributed to heterogeneity of oligodendrocytes. In the tract region oligodendrocytes would contribute longer myelin internodes, while oligodendrocytes in the nucleus laminaris region would synthesize shorter myelin internodes. Not only length of myelin internodes differs, but also along the same axon unmyelinated areas between two internodes may vary. This is an interesting contribution since all these differences contribute to differential conduction velocity regulating ipsilateral and contralateral innervation of coincidence detector neurons.

Comments on revised version:

This revised version is in large improved and the responses to reviewers' comments are generally relevant. However, the response regarding pre-nodes is not satisfactory. I understand that the authors prefer to avoid further experimentations, but I think this is an important point that needs to be clarified. Exploring stages between E12 and E15 are therefore of importance. When carefully examining some of the figures (Fig. 1E or 2D) I think that at E15 they may well be pre-nodes formation prior to myelin deposition, on structure the authors considered to be heminodes. To be convincing they should use double or triple labeling with, in addition to the nodal proteins (ankG and/or Nav pan), a good myelin marker such as antiPLP. The rat monoclonal developed by late Pr Ikenaka would give a sharper staining than the anti MAG they used. (I assume the clone must still be available in Okazaki).

https://doi.org/10.7554/eLife.106415.2.sa1

Author response:

The following is the authors' response to the original reviews

> ***Reviewer #1:***
>
> *Evidence, reproducibility and clarity*
>
> *The manuscript by Egawa and colleagues investigates differences in nodal spacing in an avian auditory brain stem circuit. The results are clearly presented and data are of very high quality. The authors make two main conclusions:*
>
> *(1) Node spacing, i.e. internodal length, is intrinsically specified by the oligodendrocytes in the region they are found in, rather than axonal properties (branching or diameter).*
>
> *(2) Activity is necessary (we don't know what kind of signaling) for normal numbers of oligodendrocytes and therefore the extent of myelination.*
>
> *These are interesting observations, albeit phenomenon. I have only a few criticisms that should be addressed:*
>
> *(1) The use of the term 'distribution' when describing the location of nodes is confusing. I think the authors mean rather than the patterns of nodal distribution, the pattern of*

> *nodal spacing. They have investigated spacing along the axon. I encourage the authors to substitute node spacing or internodal length for node distribution.*

Thanks for your suggestion to avoid confusion. We used the phrase "nodal spacing" instead of "nodal distribution" throughout the revised manuscript.

> *(2) In Seidl et al. (J Neurosci 2010) it was reported that axon diameter and internodal length (nodal spacing) were different for regions of the circuit. Can the authors help me better understand the difference between the Seidl results and those presented here?*

As a key distinction, our study focuses specifically on the main trunk of the contralateral projection of NM axons. This projection features a sequential branching structure known as the delay line, where collateral branches form terminal arbors and connect to the ventral dendritic layer of NL neurons. This structural organization plays a critical role in influencing the dynamic range of ITD detection by regulating conduction delays along the NM axon trunk.

The study by Seidl et al. (2010) is a pioneering work that measured diameter of NM axon using electron microscopy, providing highly reliable data. However, due to the technical limitations of electron microscopy, which does not allow for the continuous tracing of individual axons, it is not entirely clear whether the axons measured in the ventral NL region correspond to terminal arbors of collateral branches or the main trunk of NM axons (see Figure 9E, F in their paper). Instead, they categorized axon diameters based on their distance from NL cell layer, showing that axon diameter increases distally (see Figure 9G in their paper). Notably, the diameters of ventral axons located more than 120 μm away from the NL cell layer is almost identical to those in the midline.

As illustrated in our Figure 4D and Supplementary Video 2, the main trunk of the contralateral NM projection is predominantly located in these distal regions. Therefore, our findings complement those of Seidl et al. (2010) rather than contradicting them. We made this point as clear as possible in text (page 7, line 3).

> *(3) The authors looked only in very young animals - are the results reported here applicable only to development, or does additional refinement take place with aging?*

In this study, we examined chick embryos from E9 to just before hatching (E21) and post-hatch chicks up to P9. Chickens begin to perceive sound around E12 and possess sound localization abilities at the time of hatching (Grier et al., 1967) (added to page 4, line 9). Therefore, by E21, the sound localization circuit is largely established.

On the other hand, additional refinement of the circuit with aging is certainly possible. A key cue for sound localization, interaural time difference (ITD), depends on the distance between the two ears, which increases as the animal grows. As shown in Figure 2G, internodal length increased by approximately 20% between E18 and P9 while maintaining regional differences. Given that NM axons are nearly fully myelinated by E21 (Figure 4D, 6C), this suggests that myelin extends in proportion to the overall growth of the head and brain volume. We described this possibility in text (page 5, line 21)

Thus, our study covers not only the early stages of myelination but also the post-functional maturation in the sound localization circuit.

> *(4) The fact that internodal length is specified by the oligodendrocyte suggests that activity may not modify the location of nodes of Ranvier - although again, the authors have only looked during early development. This is quite different than this reviewer's original thoughts - that activity altered internodal length and axon diameter. Thus, the*

> *results here argue against node plasticity. The authors may choose to highlight this point or argue for or against it based on results in adult birds?*

In this study, we demonstrated that although vesicular release did not affect internodal length, it selectively promoted oligodendrogenesis, thereby supporting the full myelination and hence the pattern of nodal spacing along the NM axons. We believe that this finding falls within the broader scope of 'activity-dependent plasticity' involving oligodendrocytes and nodes.

As summarized in the excellent review by Bonetto et al. (2021), activity-dependent plasticity in oligodendrocytes encompasses a wide range of phenomena, not limited to changes in internodal length but also including oligodendrogenesis. Moreover, the effects of neuronal activity are not uniform but likely depend on the diversity of both neurons and oligodendrocytes. For example, in the mouse visual cortex, activity-dependent myelination occurs in interneurons but not in excitatory neurons (Yang et al., 2020). Additionally, expression of TeNT in axons affected myelination heterogeneously in zebrafish; some axons were impaired in myelination and the others were not affected at all (Koudelka et al., 2016). In the mouse corpus callosum, neuronal activity influences oligodendrogenesis, which in turn facilitates adaptive myelination (Gibson et al., 2014).

Thus, rather than refuting the role of activity-dependent plasticity in nodal spacing, our findings emphasize the diversity of underlying regulatory mechanisms. We described these explicitly in text (page 10, line 18).

> *Significance*
>
> *This paper may argue against node plasticity as a mechanism for tuning of neural circuits. Myelin plasticity is a very hot topic right now and node plasticity reflects myelin plasticity. this seems to be a circuit where perhaps plasticity is NOT occurring. That would be interesting to test directly. One limitation is that this is limited to development.*

This paper does not argue against node plasticity, but rather demonstrates that oligodendrocytes in the NL region exhibit a form of plasticity; they proliferate in response to vesicular release from NM axons, yet do not undergo morphological changes, ensuring adequate oligodendrocyte density for the full myelination of the auditory circuit. Thus, activity-dependent plasticity involving oligodendrocytes would contributes in various ways to each neural circuit, which is presumably attributed to the fact that myelination is driven by complex multicellular interactions between diverse axons and oligodendrocytes. Oligodendrocytes are known to exhibit heterogeneity in morphology, function, responsiveness, and gene profiles (Foerster et al., 2019; Sherafat et al., 2021; Osanai et al., 2022; Valihrach et al., 2022), but functional significance of this heterogeneity remains largely unclear. This paper also provides insight into how oligodendrocyte heterogeneity may contribute to the fine-tuning of neural circuit function, adding further value to our findings. Importantly, our study covers the wide range of development in the sound localization circuit, from the pre-myelination (E9) to the postfunctional maturation (P9), revealing how the nodal spacing pattern along the axon in this circuit emerges and matures.

> ***Reviewer #2:***
>
> *Evidence, reproducibility and clarity*
>
> *Egawa et al describe the developmental timeline of the assembly of nodes of Ranvier in the chick brainstem auditory circuit. In this unique system, the spacing between nodes varies significantly in different regions of the same axon from early stages, which the authors suggest is critical for accurate sound localization. Egawa et al set out to determine which factors regulate this differential node spacing. They do this by using*

> *immunohistological analyses to test the correlation of node spacing with morphological properties of the axons, and properties of oligodendrocytes, glial cells that wrap axons with the myelin sheaths that flank the nodes of Ranvier. They find that axonal structure does not vary significantly, but that oligodendrocyte density and morphology varies in the different regions traversed by these axons, which suggests this is a key determinant of the region-specific differences in node density and myelin sheath length. They also find that differential oligodendrocyte density is partly determined by secreted neuronal signals, as (presumed) blockage of vesicle fusion with tetanus toxin reduced oligodendrocyte density in the region where it is normally higher. Based on these findings, the authors propose that oligodendrocyte morphology, myelin sheath length, and consequently nodal distribution are primarily determined by intrinsic oligodendrocyte properties rather than neuronal factors such as activity.*
>
> *Major points, detailed below, need to be addressed to overcome some limitations of the study.*
>
> *Major comments:*
>
> *(1) It is essential that the authors validate the efficiency of TeNT to prove that vesicular release is indeed inhibited, to be able to make any claims about the effect of vesicular release on oligodendrogenesis/myelination.*

eTeNT is a widely used genetically encoded silencing tool and constructs similar to the one used in this study have been successfully applied in primates and rodents to suppress target behaviors via genetic dissection of specific pathways (Kinoshita et al., 2012; Sooksawate et al., 2013). However, precisely quantifying the extent of vesicular release inhibition from NM axons in the brainstem auditory circuit is technically problematic.

One major limitation is that while A3V efficiently infects NM neurons, its transduction efficiency does not reach 100%. In electrophysiological evaluations, NL neurons receive inputs from multiple NM axons, meaning that responses may still include input from uninfected axons. Additionally, failure to evoke synaptic responses could either indicate successful silencing or failure to stimulate NM axons, making a clear distinction difficult. Furthermore, unlike in motor circuits, we cannot assess the effect of silencing by observing behavioral outputs.

Thus, we instead opted to quantify the precise expression efficiency of GFP-tagged eTeNT in the cell bodies of NM neurons. The proportion of NM neurons expressing GFP-tagged eTeNT was 89.7 ± 1.6% (N = 6 chicks), which is consistent with previous reports evaluating A3V transduction efficiency in the brainstem auditory circuit (Matsui et al., 2012). These results strongly suggest that synaptic transmission from NM axons was globally silenced by eTeNT at the NL region. We described these explicitly in text (page 8, line 2).

> *(2) Related to 1, can the authors clarify if their TeNT expression system results in the whole tract being silenced? It appears from Fig. 6 that their approach leads to sparse expression of TeNT in individual neurons, which enables them to measure myelination parameters. Can the authors discuss how silencing a single axon can lead to a regional effect in oligodendrocyte number?*

Figure 6D depicts a representative axon selected from a dense population of GFP-positive axons in a 200-μm-thick slice after A3V-eTeNT infection to bilateral NM. As shown in Supplementary Video 1 and 2, densely labeled GFP-positive axons can be traced along the main trunk. To prevent any misinterpretation, we have revised the description of Figure 6 in the main text and Figure legend (page 31, line 9), and stated the A3V-eTeNT infection efficiency was 89.7 ± 1.6% in NM neurons, as mentioned above. Based on this efficiency, we interpreted that the global occlusion of vesicular release from most of the NM axons altered

the pericellular microenvironment of the NL region, which led to the regional effect on the oligodendrocyte density.

On the other hand, your question regarding whether sparse expression of eTeNT still has an effect is highly relevant. As we also discussed in our reply to comment 4 by Reviewer #1, the relationship between neuronal activity and oligodendrocytes is highly diverse. In some types of axons, vesicular release is essential for normal myelination, and this process was disrupted by TeNT (Koudelka et al., 2016), suggesting that direct interaction with oligodendrocytes via vesicle release may actively promote myelination in these types of axons.

To clarify whether the phenotype observed in Figure 6 arises from changes in the pericellular microenvironment at the NL region or from the direct suppression of axon-oligodendrocyte interactions, we included a new Supplementary Figure (Figure 6—figure supplement 1). In this figure, we evaluated the node formation on the axon sparsely expressing eTeNT by electroporation into the unilateral NM. The results showed that sparse eTeNT expression did not increase the percentages of heminodes or unmyelinated segments. This finding supports our conclusion that the increased unmyelinated segments by A3V-eTeNT resulted from impaired synaptic transmission at NM terminals and subsequent alterations of pericellular microenvironment at the NL region.

> *(3) The authors need to fully revise their statistical analyses throughout and supply additional information that is needed to assess if their analyses are adequate:*

Thank you for your valuable suggestions to improve the rigor of our statistical analyses. We have reanalyzed all statistical tests using R software. In the revised Methods section and Figure Legends, we have clarified the rationale for selecting each statistical test, specified which test was used for each figure, and explicitly defined both n and N. After reevaluation with the Shapiro-Wilk test, we adjusted some analyses to non-parametric tests where appropriate. However, these adjustments did not alter the statistical significance of our results compared to the original analyses.

> *(3.1) the authors use a variety of statistical tests and it is not always obvious why they chose a particular test. For example, in Fig. 2G they chose a Kruskal-Wallis test instead of a two-way ANOVA or MannWhitney U test, which are much more common in the field. What is the rationale for the test choice?*

We have revised the explanation of our statistical test choices to provide greater clarity and precision. For example, in Figure 2G, we first assessed the normality of the data in each of the four groups using the Shapiro-Wilk test, which revealed that some datasets did not follow a normal distribution. Given this, we selected the Kruskal-Wallis test, a commonly used non-parametric test for comparisons across three or more groups. Since the Kruskal-Wallis test indicated a significant difference, we conducted a post hoc Steel-Dwass test to determine which specific group comparisons were statistically significant.

> *(3.2) in some cases, the choice of test appears wholly inappropriate. For example, in Fig. 3H-K, an unpaired t-test is inappropriate if the two regions were analysed in the same samples. In Fig. 5, was a ttest used for comparisons between multiple groups in the same dataset? If so, an ANOVA may be more appropriate.*

In the case of Figures 3H-K, we compared oligodendrocyte morphology between regions. However, since the number of sparsely labeled oligodendrocytes differs both between regions and across individual samples, there is no strict correspondence between paired measurements. On the other hand, in Figures 5B, C, and E, we compared the density of

labeled cells between regions within the same slice, establishing a direct correspondence between paired data points. For these comparisons, we appropriately used a paired t-test.

> *(3.3) in some cases, the authors do not mention which test was used (Fig 3: E-G no test indicated, despite asterisks; G/L/M - which regression test that was used? What does r indicate?)*

We have specified the statistical tests used for each figure in the Methods section and Figure Legends for better clarity. Additionally, we have revised the descriptions for Figure 4G, L, and M and their corresponding Figure Legends to explicitly indicate that Spearman's rank correlation coefficient (r_s) was used for evaluation.

> *(3.4) more concerningly, throughout the results, data may have been pseudo-replicated. t-tests and ANOVAs assume that each observation in a dataset is independent of the other observations. In figures 1-4 and 6 there is a very large "n" number, but the authors do not indicate what this corresponds to. This leaves it open to interpretation, and the large values suggest that the number of nodes, internodal segments, or cells may have been used. These are not independent experimental units, and should be averaged per independent biological replicate - i.e. per animal (N).*

We have now clarified what "n" represents in each figure, as well as the number of animals (N) used in each experiment, in the Figure Legends.

In this study, developmental stages of chick embryos were defined by HH stage (Hamburger and Hamilton, 1951), minimizing individual variability. Additionally, since our study focuses on the distribution of morphological characteristics of individual cells, averaging measurements per animal would obscure important cellular-level variability and potentially mislead interpretation of data. Furthermore, we employed a strategy of sparse genetic labeling in many experiments, which naturally results in variability in the number of measurable cells per animal. Given the clear distinctions in our data distributions, we believe that averaging per biological replicate is not essential in this case.

To further ensure the robustness of our statistical analysis, data presented as boxplots were preliminarily assessed using PlotsOfDifferences, a web-based application that calculates and visualizes effect sizes and 95% confidence intervals based on bootstrapping (https://huygens.science.uva.nl/PlotsOfDifferences/; https://doi.org/10.1101/578575). Effect sizes can serve as a valuable alternative to p-values (Ho, 2018; https://www.nature.com/articles/s41592019-0470-3). The significant differences reported in our study are also supported by clear differences in effect sizes, ensuring that our conclusions remain robust regardless of the statistical approach used.

If requested, we would be happy to provide PlotsOfDifferences outputs as supplementary source data files, similar to those used in eLife publications, for each figure.

> *(3.5) related to the pseudo-replication issue, can the authors include individual datapoints in graphs for full transparency, per biological replicates, in addition or in alternative to bar-graphs (e.g. Fig. 5 and 6).*

We have now incorporated individual data points into the bar graphs in Figures 5 and 6.

> *(4) The main finding of the study is that the density of nodes differs between two regions of the chicken auditory circuit, probably due to morphological differences in the respective oligodendrocytes. Can the authors discuss if this finding is likely to be specific to the bird auditory circuit?*

The morphological differences of oligodendrocytes between white and gray matter are well established (i.e. shorter myelin at gray matter), but their correspondence with the nodal spacing pattern along the long axonal projections of cortical neurons is not well understood. Future research may find similarities with our findings. Additionally, as mentioned in the final section of the Discussion, the mammalian brainstem auditory circuit is functionally analogous to the avian ITD circuit. Regional differences in nodal spacing along axons have also been observed in the mammalian system, raising the important question of whether these differences are supported by regional heterogeneity in oligodendrocytes. Investigating this possibility will facilitate our understanding of the underlying logic and mechanisms for determining node spacing patterns along axons, as well as provide valuable insights into evolutionary convergence in auditory processing mechanisms. We described these explicitly in text (page 11, line 34).

> *(5) Provided the authors amend their statistical analyses, and assuming significant differences remain as shown, the study shows a correlation (but not causation) between node spacing and oligodendrocyte density, but the authors did not manipulate oligodendrocyte density per se (i.e. cell-autonomously). Therefore, the authors should either include such experiments, or revise some of their phrasing to soften their claims and conclusions. For example, the word "determine" in the title could be replaced by "correlate with" for a more accurate representation of the work. Similar sentences throughout the main text should be amended.*

As you summarized in your comment, our results demonstrated that A3V-eTeNT suppressed oligodendrogenesis in the NL region, leading to a reduction in oligodendrocyte density (Figures 6L, M), which caused the emergence of unmyelinated segments. While this is an indirect manipulation of oligodendrocyte density, it nonetheless provides evidence supporting a causal relationship between oligodendrocyte density and nodal spacing.

The emergence of unmyelinated segments at the NL region further suggests that the myelin extension capacity of oligodendrocytes differs between regions, highlighting regional differences in intrinsic properties of oligodendrocyte as the most prominent determinant of nodal spacing variation. However, as you correctly pointed out, our findings do not establish direct causation.

In the future, developing methods to artificially manipulate myelin length could provide a more definitive demonstration of causality. Given these considerations, we have modified the title to replace "determine" with "underlie", ensuring that our conclusions are presented with appropriate nuance.

> *(6) The authors fail to introduce, or discuss, very pertinent prior studies, in particular to contextualize their findings with:*
>
> *(6.1) known neuron-autonomous modes of node formation prior to myelination, e.g. Zonta et al (PMID 18573915); Vagionitis et al (PMID 35172135); Freeman et al (PMID 25561543)*
>
> *(6.2) known effects of vesicular fusion directly on myelinating capacity and oligodendrogenesis, e.g. Mensch et al (PMID 25849985)*
>
> *(6.3) known correlation of myelin length and thickness with axonal diameter, e.g. Murray & Blakemore (PMID 7012280); Ibrahim et al (PMID 8583214); Hildebrand et al (PMID 8441812).*
>
> *(6.4) regional heterogeneity in the oligodendrocyte transcriptome (page 9, studies summarized in PMID 36313617)*

Thank you for your insightful suggestions. We have incorporated the relevant references you provided and revised the manuscript accordingly to contextualize our findings within the existing literature.

> *Minor comments:*
>
> *(7) Can the authors amend Fig. 1G with the correct units of measurement, not millimetres.*

Response:

Thank you for your suggestion. We have corrected the units in Figure 1G to μm

> *(8) The Olig2 staining in Fig 2C does not appear to be nuclear, as would be expected of a transcription factor and as is well established for Olig2, but rather appears to be excluded from the nucleus, as it is in a ring or donut shape. Can the authors comment on this?*

Oligodendrocytes and OPCs have small cell bodies, often comparable in size to their nuclei. The central void in the ring-like Olig2 staining pattern appears too small to represent the nucleus. Additionally, a similar ring-like appearance is observed in BrdU labeling (Figure 5G), suggesting that this staining pattern may reflect nuclear morphology or other structural features.

> *Significance*
>
> *In our view the study tackles a fundamental question likely to be of interest to a specialized audience of cellular neuroscientists. This descriptive study is suggestive that in the studied system, oligodendrocyte density determines the spacing between nodes of Ranvier, but further manipulations of oligodendrocyte density per se are needed to test this convincingly.*

The main finding of our study is that the primary determinant of the biased nodal spacing pattern in the sound localization circuit is the regional heterogeneity in the morphology of oligodendrocytes due to their intrinsic properties (e.g., their ability to produce and extend myelin sheaths) rather than the density of the cells. This was based on our observations that a reduction of oligodendrocyte density by A3V-eTeNT expression caused unmyelinated segments but did not increase internodal length (Figure 6), further revealing the importance of oligodendrocyte density in ensuring full myelination for the axons with short internodes. Thus, we think that our study could propose the significance of oligodendrocyte heterogeneity in the circuit function as well as in the nodal spacing using experimental manipulation of oligodendrocyte density.

> ***Reviewer #3:***
>
> *Evidence, reproducibility and clarity*
>
> *The authors have investigated the myelination pattern along the axons of chick avian cochlear nucleus. It has already been shown that there are regional differences in the internodal length of axons in the nucleus magnocellularis. In the tract region across the midline, internodes are longer than in the nucleus laminaris region. Here the authors suggest that the difference in internodal length is attributed to heterogeneity of oligodendrocytes. In the tract region oligodendrocytes would contribute longer myelin internodes, while oligodendrocytes in the nucleus laminaris region would synthesize shorter myelin internodes. Not only length of myelin internodes differs, but also along*

> *the same axon unmyelinated areas between two internodes may vary. This is an interesting contribution since all these differences contribute to differential conduction velocity regulating ipsilateral and contralateral innervation of coincidence detector neurons. However, the demonstration falls rather short of being convincing. I have some major concerns:*
>
> *(1) The authors neglect the possibility that nodal cluster may be formed prior to myelin deposition. They have investigated stages E12 (no nodal clusters) and E15 (nodal cluster plus MAG+ myelin). Fig. 1D is of dubious quality. It would be important to investigate stages between E12 and E15 to observe the formation of pre-nodes, i.e., clustering of nodal components prior to myelin deposition.*

Thank you for your insightful comment regarding the potential role of pre-nodal clusters in determining internodal length. Indeed, studies in zebrafish have suggested that pre-nodal clustering of node components prior to myelination may prefigure internodal length (Vagionitis et al., 2022). We have incorporated a discussion on whether such pre-nodal clusters could contribute to regional differences in nodal spacing in our manuscript (page 9, line 35).

Whether pre-nodal clusters are detectable before myelination appears to depend on neuronal subpopulation (Freeman et al., 2015). To investigate the presence of pre-nodal clusters along NM axons in the brainstem auditory circuit, we previously attempted to visualize AnkG signals at E13 and E14. However, we did not observe clear structures indicative of pre-nodal clusters; instead, we only detected sparse fibrous AnkG signals with weak Nav clustering at their ends, consistent with hemi-node features. This result does not exclude the possibility of pre-nodal clusters on NM axons, as the detection limit of immunostaining cannot be ruled out. In brainstem slices, where axons are densely packed, nodal molecules are expressed at low levels across a wide area, leading to a high background signal in immunostaining, which may mask weak pre-nodal cluster signals prior to myelination. Regarding the comment on Figure 1D, we assume you are referring to Figure 2D based on the context. The lack of clarity in the high-magnification images in Figure 2D results from both the high background signal and the limited penetration of the MAG antibody. Furthermore, we are unable to verify Neurofascin accumulation at pre-nodal clusters, as there is currently no commercially available antibody suitable for use in chickens, despite our over 20 years of efforts to identify one for AIS research. Therefore, current methodologies pose significant challenges in visualizing pre-nodal clusters in our model. Future advancements, such as exogenous expression of fluorescently tagged Neurofascin at appropriate densities or knock-in tagging of endogenous molecules, may help overcome these limitations.

However, a key issue to be discussed in this study is not merely the presence or absence of prenodal clusters, but rather whether pre-nodal clusters—if present—would determine regional differences in internodal length. To address this possibility, we have added new data in Figure 6I, measuring the length of unmyelinated segments that emerged following A3V-eTeNT expression.

If pre-nodal clusters were fixed before myelination and predetermined internodal length, then the length of unmyelinated segments should be equal to or a multiple of the typical internodal length. However, our data showed that unmyelinated segments in the NL region were less than half the length of the typical NL internodal length, contradicting the hypothesis that fixed pre-nodal clusters determine internodal length along NM axons in this region.

> *(2) The claim that axonal diameter is constant along the axonal length need to be demonstrated at the EM level. This would also allow to measure possible regional differences in the thickness of the myelin sheath and number of myelin wraps.*

As mentioned in our reply to comment 2 by Reviewer #1, the diameter of NM axons was already evaluated using electron microscopy (EM) in the pioneering study by Seidl et al., (2010). Additionally, EM-based analysis makes it difficult to clearly distinguish between the main trunk of NM axons and thin collateral branches at the NL region. Accordingly, we did not do the EM analysis in this revision.

In Figure 4, we used palGFP, which is targeted to the cell membrane, allowing us to measure axon diameter by evaluating the distance between two membrane signal peaks. This approach minimizes the influence of the blurring of fluorescence signals on diameter measurements. Thus, we believe that our method is sufficient to evaluate the relative difference in axon diameters between regions and hence to show that axon diameter is not the primary determinant of the 3-fold difference in internodal length between regions.

> *(3) The observation that internodal length differs is explain by heterogeneity of sources of oligodendrocyte is not convincing. Oligodendrocytes a priori from the same origin remyelinate shorter internode after a demyelination event.*

The heterogeneity in oligodendrocyte morphology would reflect differences in gene profiles, which, in turn, may arise from differences in their developmental origin and/or pericellular microenvironment of OPCs. We made this point as clear as possible in Discussion (page 9, line 21).

> *Significance*
>
> *The authors suggest that the difference in internodal length is attributed to heterogeneity of oligodendrocytes. In the tract region oligodendrocytes would contribute longer myelin internodes, while oligodendrocytes in the nucleus laminaris region would synthesize shorter myelin internodes. Not only length of myelin internodes differs, but also along the same axon unmyelinated areas between two internodes may vary. This is an interesting contribution since all these differences contribute to differential conduction velocity regulating ipsilateral and contralateral innervation of coincidence detector neurons.*

https://doi.org/10.7554/eLife.106415.2.sa0